THE UNIVERSITY OF WISCONSIN—MILWAUKEE

CENTER
FOR
GREAT LAKES STUDIES

MILWAUKEE, WISCONSIN 53201 U.S.A.

SPECIAL REPORT NO. 20

A Normal Mode Method for Predicting Storm Surges on a Lake

by

DAVID J. SCHWAB

Center for Great Lakes Studies
The University of Wisconsin--Milwaukee
Milwaukee, Wisconsin, USA, 53201

November 1975

TABLE OF CONTENTS

LIST OF FIGURES

List of Figures (continued)

LIST OF TABLES

ACKNOWLEDGEMENTS

This research would not have been possible without the encouragement and guidance of my advisor, Dr. D. B. Rao. This work was supported partially by the Oceanography Section of the National Science Foundation through Grant No. GA-32204 and partially by the Center for Great Lakes Studies at The University of Wisconsin--Milwaukee. Special thanks to Kathie Lehnhardt for typing and assembling the manuscript and to Mr. Ratko J. Ristic for drafting assistance.

A NORMAL MODE METHOD FOR
PREDICTING STORM SURGES ON A LAKE

by

DAVID JOHN SCHWAB

ABSTRACT

A mathematical procedure for determining the two-dimensional time-dependent response of a rotating lake with arbitrary topography is presented. The procedure depends on prior knowledge of the normal modes of oscillation of the lake. These may be found numerically for an arbitrary lake by the method of Rao and Schwab (1974). The space-dependent part of the forced solution is represented by an expansion in terms of the spectrum of normal modes. This results in a system of uncoupled first-order inhomogeneous differential equations which depend only on time and can be solved simply and efficiently by implicit numerical integration. The normal mode method avoids the problem of grid-dispersion inherent in the traditional approach of direct finite difference integration of the governing equations on a numerical space-time grid. It is also more economical in terms of computation time than the finite difference method. Furthermore, the normal mode method provides physical insight by determining exactly how the total energy of the lake is distributed among the individual modes.

Results of the application of this technique to an ideal rectangular basin compare well with the solution by a finite difference technique. Favorable comparisons are also obtained for a natural basin, Lake Ontario, subjected to a uniform wind stress and a natural wind stress. The computational efficiency of the normal mode technique is evident in all cases. An Appendix compares the results of these two-dimensional methods to the solution of the channel equations for Lake Ontario with uniform wind stress.

CHAPTER ONE

INTRODUCTION

When a lake is subjected to external forcing in the form of wind stress, atmospheric pressure gradients, or tidal forcing, energy is transferred to the lake and is manifest on a variety of scales. The bulk of this energy is absorbed in coordinated motions of the entire water mass. For theoretical as well as practical reasons there is interest in predicting these large-scale (whole basin) motions in a lake when an external force is applied.

One of the most conspicuous large-scale manifestations of the energy in a lake during late fall and early winter when stratification is unimportant and atmospheric forcing is at its strongest, is the displacement of the free surface from its equilibrium position caused by the passage of a storm or pressure front across the lake. Commonly referred to as a "storm surge", this displacement may amount to several meters in severe cases on large lakes. Typical time scales of such storm passages are about 48 hours.

Analytical solutions to the mathematical storm surge problem have been sought by introducing such assumptions as one-dimensionality, constant depth, or rectangular geometry. For example, Proudman (1953) considers the response of a narrow rectangular basin to strictly periodic forcing. Lamb (1932) offers solutions for periodic forcing in circular and rectangular basins. The method of characteristics is employed by Rao (1967) to find the response of a rectangular basin with uniform depth to a moving stress band. Analytical treatment, however, is incapable of dealing with

natural topography and wind conditions. Consequently the system of governing differential equations has been formulated in finite difference form and applied at discrete points on a numerical grid which can take into account the actual topography of the water body. Welander (1961) cites examples of such calculations on the North Sea, the Baltic Sea, and Lake Michigan. Lauwerier and Damste (1963) also present results for the North Sea. The double Richardson lattice scheme used by Platzman (1963)on Lake Erie is now considered the standard method for storm surge prediction. A similar procedure is incorporated in the multilayered model of Simons (1973). In the time integration aspect of the finite difference system, if an explicit integration technique is employed, the resolution of the horizontal grid restricts the size of the maximum time increment for which the system will be stable. Implicit integration imposes no limit on the time step for computational stability, but the nature of the dynamical equations requires the inversion of an often prohibitively large matrix. The space-time finite difference system can also become computationally unstable through the problem of lattice-dispersion (see Platzman 1963, Simons 1971).

The response of a lake to arbitrary forcing can be decomposed into a combination of the free modes of oscillation of the basin, with the amplitude of each mode determined by the forcing function. Lauwerier (1961) used this principle to represent the forced solution for a rectangular bay as the sum of two Kelvin waves and an infinite series of Poincare waves, which are the basis of the free solutions in a rectangular bay. In a basin with arbitrary topography the Kelvin and Poincare waves are no longer appropriate.

The free solutions are the normal modes of oscillation of the lake. These may be found numerically for a natural basin by several methods (Hamblin 1972, Platzman 1972 and 1974, Rao and Schwab 1974). The method of Rao and Schwab (1974) is employed here to obtain the spectrum of normal modes.

The normal modes represent the homogeneous solutions of the dynamical equations. Theoretically there exists an infinite spectrum of normal modes. When forcing is applied the equations become inhomogeneous and the particular solution can be determined by expansion in terms of the normal modes with time-dependent expansion coefficients, as, for example, done by Reid (1958) in a study dealing with edge wave generation on a sloping shelf. For a given type of forcing the normal mode expansion may be tailored to fit the problem by retaining only the modes that are expected to acquire energy from the forcing agent. The normal mode expansion automatically satisfies the space-dependent aspect of the problem. Each of the expansion coefficients is found to satisfy a first-order inhomogeneous ordinary differential equation in time alone, which can be solved by standard numerical techniques. For these equations implicit integration does not require a matrix inversion since the system is uncoupled. This type of analysis has been performed for some ideal cases by Rao (1974).

The governing equations and pertinent assumptions will be presented in Chapter 2. Chapter 3 will deal with the construction of the normal modes. Chapter 4 explains the spectral expansion and time integration for determining the forced response. A brief discussion of a finite difference space-time method and a comparison of results with the normal mode method

follow in Chapter 5. The spectral method is applied to an actual storm on Lake Ontario in Chapter 6, and Chapter 7 summarizes the results.

The elongated shape of Lake Ontario suggests that the one-dimensional channel equations may provide a sufficiently accurate solution for storm surge prediction. A comparison of the one-dimensional and two-dimensional solutions for a uniform wind along the channel axis is discussed in Appendix B.

CHAPTER TWO

DYNAMICAL EQUATIONS

In the context of large-scale oscillations in homogeneous lakes, the water depth is much smaller than the horizontal scale of the oscillation. This is the basic assumption of shallow water theory, which permits the vertical acceleration to be ignored. The water mass is then in hydrostatic equilibrium and the horizontal velocity is independent of depth. The equation of continuity may be integrated in the vertical. The horizontal velocity and and free surface displacement are regarded as perturbations on an equilibrium state of rest and quantities nonlinear in these terms are disregarded. Because of the space and time scales involved, bottom friction and horizontal diffusion of momentum are not important but the modification of the velocity by the earth's rotation must be considered. These approximations are quite standard for the storm surge problem and are thoroughly discussed in Platzman (1958).

Consider a cartesian coordinate system with the origin at the undisturbed free surface of the lake with the z-axis pointing upward. The lake is rotating about the vertical axis with angular frequency $f/2$. The coriolis parameter, f, is related to the angular frequency of rotation of the earth, Ω, and the latitude, θ, by $f = 2\,\Omega \sin\theta$. The depth is given by $h(x, y)$. The constant of apparent gravitational attraction is g. The dynamical equations may be written as:

$$\frac{\partial |M}{\partial t} - f[|M] = -gh\,\nabla\eta + \gamma \qquad [2.1a]$$

$$\frac{\partial \eta}{\partial t} + \nabla \cdot |M = 0 \qquad [2.1b]$$

where $\mathbf{M} = (M, N)$ is the transport vector

$$\mathbf{M} = \int_{-h}^{\eta} \mathbf{v} dz$$

with $\mathbf{v}$ the horizontal velocity vector. The displacement of the free surface from its equilibrium level is η, t is time, ∇ is the horizontal gradient operator, and [ ] is an operator which denotes the rotation of a vector 90° clockwise in the horizontal plane. $\mathcal{T}(x, y, t)$ is the prescribed forcing function. The appropriate boundary condition is:

$$\mathbf{M} \cdot \mathbf{n} = h\mathbf{v} \cdot \mathbf{n} = 0 \qquad [2.2]$$

on the shoreline. Here $\mathbf{n}$ is a vector normal to the shoreline.

The dynamical equations [2.1] and boundary condition [2.2] describe an initial-boundary value problem with prescribed values of mass transport and free surface displacement as the initial conditions and the boundary condition [2.2] of zero transport normal to the shoreline. During a storm surge the effect of wind stress and pressure gradients tends to reduce the importance of the initial conditions and after some period of time the initial conditions should be of negligible importance. Hence, the specification of the forcing functions and the topography of the lake are expected to be the primary factors in a storm surge calculation.

CHAPTER THREE

NORMAL MODES OF A LAKE

The normal modes of a lake represent the solutions to the dynamical equations [2.1] in the absence of forcing ($\mathcal{T} = 0$). Although many methods exist for determining the free modes of oscillation the most satisfactory technique for a large number of modes is that of Rao and Schwab (1974) which is adapted here.

A. Theory:

The first step in the procedure is to partition the transport vector $\mathbf{M}$ into a non-divergent and an irrotational part. This may be done because $\mathbf{M}$ is independent of depth and the boundary conditions are adiabatic. The partitioning of $\mathbf{M}$ is:

$$\mathbf{M} = \mathbf{M}^{\phi} + \mathbf{M}^{\psi} \qquad [3.1]$$

where $\mathbf{M}^{\phi}$ and $\mathbf{M}^{\psi}$ are given in terms of two scalar functions ϕ and ψ:

$$\mathbf{M}^{\phi} = h \nabla \phi$$
$$\mathbf{M}^{\psi} = -[\nabla \psi]. \qquad [3.2]$$

ϕ and ψ are the potential and stream functions for the transport field. Now $h^{-1}\mathbf{M}^{\phi}$ is irrotational and $\mathbf{M}^{\psi}$ is nondivergent.

$$\nabla \cdot [h^{-1}\mathbf{M}^{\phi}] = 0$$
$$\nabla \cdot \mathbf{M}^{\psi} = 0 \qquad [3.3]$$

The boundary condition [2.2] is satisfied by

$$\mathbf{M}^{\phi} \cdot \mathbf{n} = 0$$
$$\mathbf{M}^{\psi} \cdot \mathbf{n} = 0 \qquad [3.4]$$

or in terms of ϕ and ψ:

$$h \frac{\partial \phi}{\partial n} = O$$
$$\psi = O \qquad [3.5]$$

on the shoreline.

To determine $\mathbf{M}$, examine the divergence of the transport field and vorticity of the velocity field.

$$\nabla \cdot h \nabla \phi = -\nabla \cdot \mathbf{M}$$
$$\nabla \cdot h \nabla \psi = \nabla \cdot [h^{-1} \mathbf{M}]. \qquad [3.6]$$

If $\mathbf{M}$ is known, [3.6] represents an inhomogeneous elliptic partial differential equation with homogeneous boundary conditions [3.5]. Such a problem has a unique solution. $\mathbf{M}$, however, is unknown; but it satisfies the dynamical equations [2.1] in the absence of forcing. To determine $\mathbf{M}$, convert the governing equations [2.1] with $\mathcal{T} = O$ into conditions on ϕ and ψ and reconstruct $\mathbf{M}$ with [3.1,2].

For this purpose represent ϕ and ψ in terms of the spectra of the elliptic operators in [3.6]. That is, consider the characteristic value problems

$$\nabla \cdot h \nabla \phi_\alpha = -\lambda_\alpha \phi_\alpha,$$
$$h \frac{\partial \phi}{\partial n} \alpha = O \text{ on the boundary} \qquad [3.7a]$$

$$\nabla \cdot h^{-1} \nabla \psi_\alpha = -\mu_\alpha \psi_\alpha,$$
$$\psi_\alpha = O \text{ on the boundary} \qquad [3.7b]$$

where α is a binary index used to number the spectral components. With the more stringent boundary condition $h^{-1}\psi_\alpha = 0$, [3.7a, b] are self-adjoint. Hence, the characteristic values λ_α, μ_α are real and the associated eigenfunctions ϕ_α, ψ_α each form a complete internally orthogonal set. The orthogonality condition is chosen as

$$\int h^{-1} \mathbf{M}^{\phi}_{\alpha} \cdot \mathbf{M}^{\phi}_{\beta}\, dA = \lambda_\alpha \int \phi_\alpha \phi_\beta\, dA = gA\delta_{\alpha\beta}$$
$$\int h^{-1} \mathbf{M}^{\psi}_{\alpha} \cdot \mathbf{M}^{\psi}_{\beta}\, dA = \mu_\alpha \int \psi_\alpha \psi_\beta\, dA = gA\delta_{\alpha\beta} \qquad [3.8]$$

where A is the surface area of the lake and δ is the Kronecker delta. Also, in accordance with [3.2]

$$\mathbf{M}^{\phi}_{\alpha} = -h \nabla \phi_\alpha$$
$$\mathbf{M}^{\psi}_{\alpha} = -[\nabla \psi_\alpha]. \qquad [3.9]$$

Now define nondimensional expansion coefficients to represent $\mathbf{M}^{\phi}$ and $\mathbf{M}^{\psi}$.

$$P_\alpha = \frac{1}{gA}\int h^{-1} \mathbf{M}^{\phi}_{\alpha} \cdot \mathbf{M}^{\phi} dA = \frac{1}{gA}\int h^{-1} \mathbf{M}^{\phi}_{\alpha} \cdot \mathbf{M}\, dA$$
$$Q_\alpha = \frac{1}{gA}\int h^{-1} \mathbf{M}^{\psi}_{\alpha} \cdot \mathbf{M}^{\psi} dA = \frac{1}{gA}\int h^{-1} \mathbf{M}^{\psi}_{\alpha} \cdot \mathbf{M} dA. \qquad [3.10]$$

In view of the orthogonality condition [3.8], the sums on the right of

$$\mathbf{M}^{\phi} = \sum_\alpha P_\alpha \mathbf{M}^{\phi}_{\alpha}$$
$$\mathbf{M}^{\psi} = \sum_\alpha Q_\alpha \mathbf{M}^{\psi}_{\alpha} \qquad [3.11]$$

represent the least squares approximations to $\mathbf{M}^{\phi}$ and $\mathbf{M}^{\psi}$ when the sums span the complete spectra of [3.7].

To find a basis for the free surface displacement an examination of [2.1b] shows that η is governed by the divergent part of $\mathbb{M}$. Hence, ϕ_α form a sufficient basis for η. We define

$$\eta_\alpha = g^{-1} \lambda_\alpha^{\frac{1}{2}} \phi_\alpha \qquad [3.12]$$

so that the orthonormality relation is

$$\int \eta_\alpha \eta_\beta \, dA = A \delta_{\alpha\beta}. \qquad [3.13]$$

The expansion coefficients for η are

$$R_\alpha = \frac{1}{A} \int \eta_\alpha \eta \, dA \qquad [3.14]$$

and the expansion is

$$\eta = \sum_\alpha R_\alpha \eta_\alpha. \qquad [3.15]$$

All of the dependent variables are now represented in terms of the spectra of [3.7] by the expressions [3.11,15].

The expansions [3.11,15] are substituted for the dependent variables in the dynamical equations [2.1] with $\mathcal{T} = 0$ and the expansion coefficients are isolated by the use of the orthogonality conditions [3.8, 13] in the usual way to obtain the spectral prediction equations.

$$\begin{aligned}
&\frac{dP_\alpha}{dt} - \sum_\beta A_{\alpha\beta} P_\beta - \sum_\beta B_{\alpha\beta} Q_\beta - \nu_\alpha R_\alpha = O \\
&\frac{dQ_\alpha}{dt} - \sum_\beta C_{\alpha\beta} P_\beta - \sum_\beta D_{\alpha\beta} Q_\beta = O \\
&\frac{dR_\alpha}{dt} + \nu_\alpha P_\alpha = O.
\end{aligned} \qquad [3.16]$$

The following definitions have been introduced:

$$A_{\alpha\beta} = \left\{ |M^{\phi}_{\alpha}, [|M^{\phi}_{\beta}] \right\}, \quad B_{\alpha\beta} = \left\{ |M^{\phi}_{\alpha}, [|M^{\psi}_{\beta}] \right\}$$

$$C_{\alpha\beta} = \left\{ |M^{\psi}_{\alpha}, [|M^{\phi}_{\beta}] \right\}, \quad D_{\alpha\beta} = \left\{ |M^{\psi}_{\alpha}, [|M^{\psi}_{\beta}] \right\} \qquad [3.17]$$

where the notation $\left\{ /A, |B \right\}$ represents the inner product defined by

$$\left\{ /A, |B \right\} = \frac{1}{gA} \int fh^{-1} \, /A \cdot |B dA.$$

Note that from [3.17]

$$A_{\alpha\beta} = -A_{\beta\alpha}, \quad B_{\alpha\beta} = -C_{\beta\alpha}, \quad D_{\alpha\beta} = -D_{\beta\alpha}. \qquad [3.18]$$

In [3.17] ν_{α} is given by

$$\nu_{\alpha} = (g \lambda_{\alpha})^{\frac{1}{2}} \qquad [3.19]$$

Define now the column vectors

$$\begin{aligned} \overline{P} &= \text{col}\,(P_{\alpha}) \\ \overline{Q} &= \text{col}\,(Q_{\alpha}) \\ \overline{R} &= \text{col}\,(R_{\alpha}) \end{aligned} \qquad \overline{S} = \begin{pmatrix} \overline{P} \\ \overline{Q} \\ \overline{R} \end{pmatrix} \qquad [3.20]$$

and matrices

$$A = |Aij|, \quad B = |Bij|$$

$$C = |Cij|, \quad D = |Dij|, \quad \langle \nu \rangle = \text{diag}\,(\nu_{\alpha}). \qquad [3.21]$$

Equations [3.16] can now be written in matrix form as

$$\frac{d\bar{S}}{dt} + a\bar{S} = O \qquad [3.22]$$

where a is a square matrix

$$a = \begin{vmatrix} -A & -B & -\langle\nu\rangle \\ -C & -D & O \\ \langle\nu\rangle & O & O \end{vmatrix} \qquad [3.23]$$

The normal modes are periodic in time so let the time dependent part of $\bar{S}$ be given by $e^{i\sigma t}$ where σ is the frequency of oscillation and $i = \sqrt{-1}$. Then [3.22] becomes

$$i\sigma\bar{S} + a\bar{S} = O \quad \text{or} \quad (\sigma II - ia)\bar{S} = O \qquad [3.24]$$

with II the identity matrix. [3.24] is now in the form of a standard eigenvalue problem for the matrix ia. From [3.18] and [3.23] it is clear that the matrix ia has Hermitian symmetry. Hence, the characteristic values σ are real. The eigenvalue problem [3.24] can be solved by standard techniques for the characteristic values σ and eigenvectors $\bar{S}$. From $\bar{S}$, the definitions [3.9], and the expansions [3.11, 15] the mass transport and free surface displacement fields for the normal modes are constructed.

The normal modes for a rotating basin with non-uniform depth fall into two categories known as oscillations of the first and second class. Oscillations of the first class are induced by the gravitational potential and

have the property that their frequency of oscillation approaches the frequency of the corresponding gravitational mode in the absence of rotation as the rotation rate is reduced to zero. Oscillations of the second class depend on the potential vorticity of the water mass and their frequencies tend to zero as the rotation goes to zero. For reasons detailed in the following chapters only the spectrum of gravitational modes will be considered here.

B. Application to Lake Ontario:

For non-analytical topography the characteristic value problem [3.7] and [3.24] must be solved by numerical methods. This has been done for Lake Ontario and Lake Superior by Rao and Schwab (1974). Results for the six lowest (in terms of frequency) gravitational modes in Lake Ontario are presented in Figures 1 and 2. These figures show the phase and amplitude of the free surface displacement η. The solid lines are cotidal lines and the dashed lines are co-range lines. Write the solution for η as

$$\eta = \text{Real} \sum_{\alpha} R_{\alpha} \eta_{\alpha} e^{i\sigma t} = A(x,y) \cos(\sigma t - \Theta(x,y)).$$

The cotidal lines are isopleths of $A(x,y)$ and the co-range lines are the isopleths of $\Theta(x,y)$. The periods ($= 2\pi/\sigma$) of these six modes are given in Table 1.

Table 1. Periods of the lowest six gravitational modes in Lake Ontario.

MODE	PERIOD IN HOURS
1	5.11
2	3.11
3	2.31
4	1.87
5	1.78
6	1.46

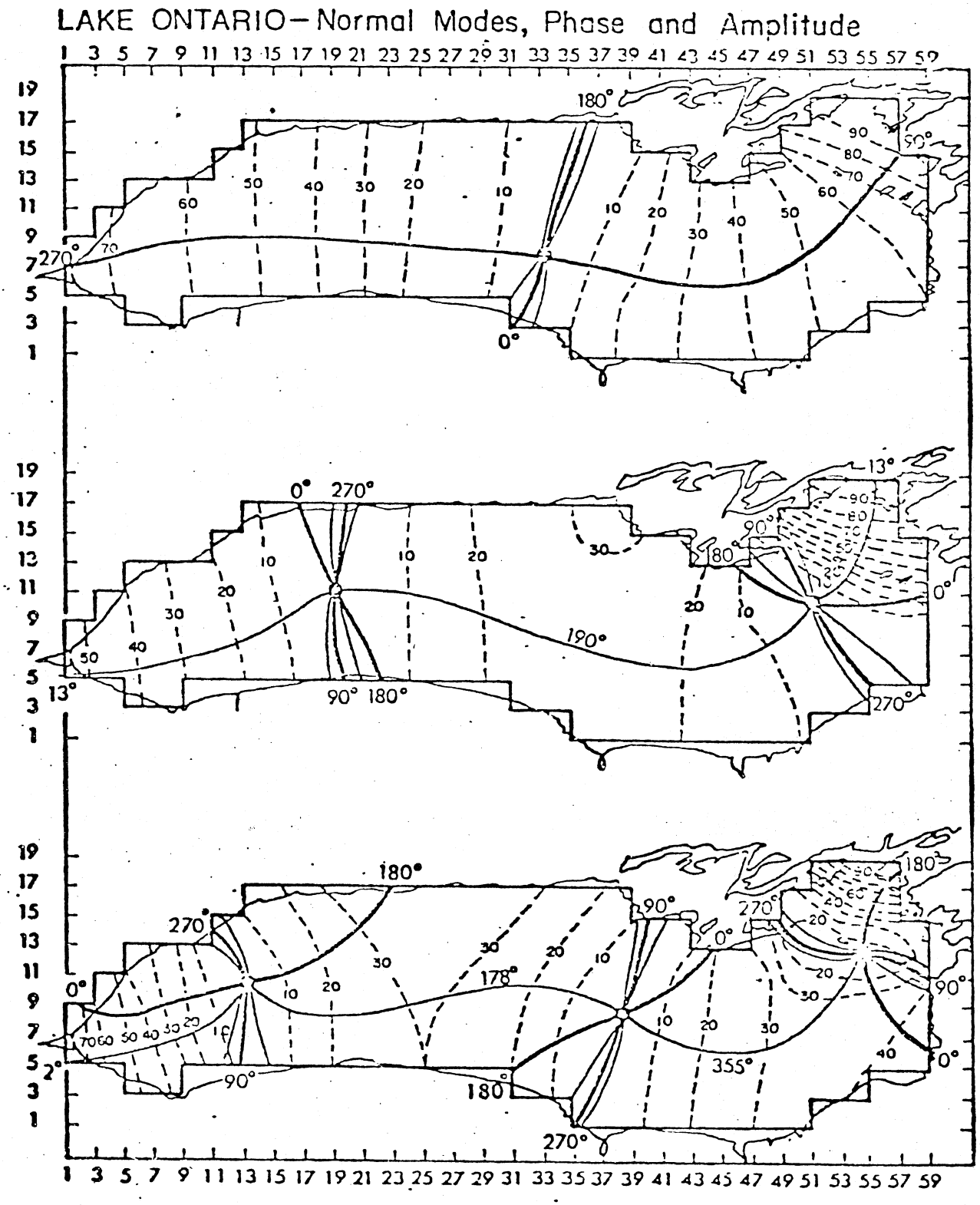

Figure 1. The first, second, and third normal modes for Lake Ontario.

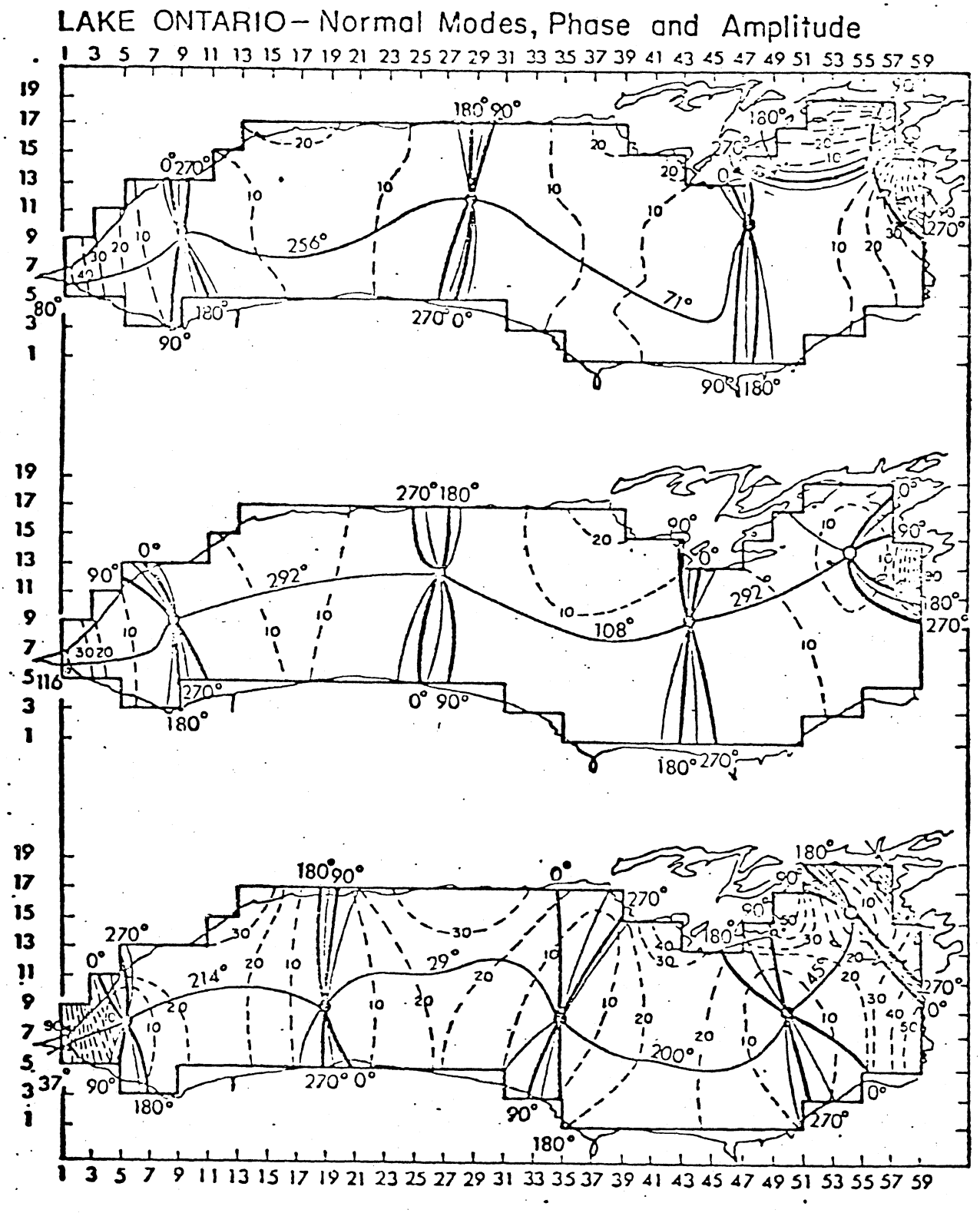

Figure 2. The fourth, fifth, and sixth normal modes for Lake Ontario.

CHAPTER FOUR

FORCED SOLUTION BY THE METHOD OF NORMAL MODES

The dynamical equations [2.1] have been solved for the unforced case ($\mathcal{L} = 0$) in the previous chapter. Let the free solutions be given by $\mathbb{M}_F$ and η_F. These can be written as

$$\mathbb{M}_F = \mathbb{M}_{j\alpha}(x, y)\, e^{i\sigma_{j\alpha} t}$$

$$\eta_F = \eta_{j\alpha}(x, y)\, e^{i\sigma_{j\alpha} t} \qquad [4.1]$$

with $M_{j\alpha}$ and $\eta_{j\alpha}$ the space dependent normal mode functions that can be found from [3.11] and [3.15]. Here α is an index that enumerates these normal modes. The subscript j has the values 1 and 2 to represent the normal mode and its complex conjugate. The complex functions $\mathbb{M}_{j\alpha}$ and $\eta_{j\alpha}$ satisfy the normal mode equations

$$i\sigma_{j\alpha}\, \mathbb{M}_{j\alpha} - f[\mathbb{M}_{j\alpha}] = -gh\, \nabla \eta_{j\alpha} \qquad [4.2a]$$

$$i\sigma_{j\alpha}\, \eta_{j\alpha} + \nabla \cdot M_{j\alpha} = O. \qquad [4.2b]$$

These functions are orthogonal in the generalized Hilbert sense. To prove this, let $\mathbb{M}^*_{k\beta}$ and $\eta^*_{k\beta}$ be the complex conjugates of the normal mode functions associated with $\sigma_{k\beta}$. They satisfy the conjugate equations of [4.2]. That is

$$-i\sigma^*_{k\beta}\, \mathbb{M}^*_{k\beta} - f[\mathbb{M}^*_{k\beta}] = -gh\, \nabla \eta^*_{k\beta} \qquad [4.3a]$$

$$-i\sigma^*_{k\beta}\, \eta^*_{k\beta} + \nabla \cdot \mathbb{M}^*_{k\beta} = O. \qquad [4.3b]$$

Multiplication of [4.2a] by $|M^*_{k\beta}/gh$,[4.2b] by $\eta^*_{k\beta}$, [4.3a] by $|M_{j\alpha}/gh$, [4.3b] by $\eta_{j\alpha}$, and addition of the resulting equations gives

$$i(\sigma^*_{k\beta} - \sigma_{j\alpha})\left(\frac{|M_{j\alpha} \cdot |M^*_{k\beta}}{gh} + \eta_{j\alpha}\,\eta^*_{k\beta}\right) = -\nabla\cdot(\eta^*_{k\beta}\,|M_{j\alpha} + \eta_{j\alpha}|M^*_{k\beta}) \qquad [4.4]$$

When [4.4] is integrated over the area of the basin the boundary condition [3.2] which satisfied by $|M_{j\alpha}$ and $|M^*_{k\beta}$ causes the right side to vanish. The result is

$$i(\sigma^*_{k\beta} - \sigma_{j\alpha})\int\left(\frac{|M_{j\alpha} \cdot |M^*_{k\beta}}{gh} + \eta_{j\alpha}\,\eta^*_{k\beta}\right) dA = 0. \qquad [4.5]$$

When $\sigma_{j\alpha} \neq \sigma^*_{k\beta}$ the integral vanishes. If $\alpha = \beta$ and $j = k$, the integrand is the sum of the squares of two real quantities and the integral is positive definite. Hence, $\sigma_{j\alpha} = \sigma^*_{j\alpha}$, which shown that the characteristic values are real. The orthonormality condition is then

$$\int\left(\frac{|M_{j\alpha} \cdot |M^*_{k\beta}}{gh} + \eta_{j\alpha}\,\eta^*_{k\beta}\right) dA = X_{j\alpha}\,\delta_{jk}\,\delta_{\alpha\beta}. \qquad [4.6]$$

$X_{j\alpha}$ is the normalization factor for the normal mode associated with $\sigma_{j\alpha}$. Now express the solution of the forced problem [2.1] as

$$|M(x,y,t) = \sum_{j=1}^{2}\sum_{\alpha} A_{j\alpha}(t)\;|M_{j\alpha}(x,y)$$

$$\eta(x,y,t) = \sum_{j=1}^{2}\sum_{\alpha} A_{j\alpha}(t)\;\eta_{j\alpha}(x,y) \qquad [4.7]$$

where $A_{j\alpha}$ is the complex time-dependent amplitude factor for the normal mode with frequency $\sigma_{j\alpha}$. Theoretically the sums in [4.7] span the entire normal mode spectrum.

Substitution of [4.7] into the dynamical equations [2.1] gives

$$\sum_{j=1}^{2} \sum_{\alpha} \frac{dA_{j\alpha}}{dt} \mathbb{M}_{j\alpha} + f \sum_{j=1}^{2} \sum_{\alpha} A_{j\alpha} [\mathbb{M}_{j\alpha}] =$$

$$-gh \sum_{j=1}^{2} \sum_{\alpha} A_{j\alpha} \eta_{j\alpha} + \mathcal{T} \qquad [4.8a]$$

$$\sum_{j=1}^{2} \sum_{\alpha} \frac{dA_{j\alpha}}{dt} \eta_{j\alpha} + \sum_{j=1}^{2} \sum_{\alpha} A_{j\alpha} \nabla \cdot \mathbb{M}_{j\alpha} = 0. \qquad [4.8b]$$

Multiply [4.8a] by $\mathbb{M}^{*}_{k\beta}/gh$, [4.8b] by $\eta^{*}_{k\beta}$, [4.3a] by $\mathbb{M}/gh$, and [4.3b] by η where $\mathbb{M}$ and η are taken from [4.7]. Addition of the resulting equations and integration over the area of the basin with the use of the orthonormality condition [4.6] gives

$$X_{j\alpha}\left(\frac{dA_{j\alpha}}{dt} + i\sigma_{j\alpha} A_{j\alpha} \right) = \int \frac{\mathcal{T} \cdot \mathbb{M}^{*}_{j\alpha}}{gh} \, dA$$

or

$$\frac{dA_{j\alpha}}{dt} + i\sigma_{j\alpha} A_{j\alpha} = \frac{1}{X_{j\alpha}} \int \frac{\cdot \mathbb{M}^{*}_{j\alpha}}{gh} \, dA. \qquad [4.9]$$

Since the forcing function $\mathcal{T}$ is a prescribed quantity, [4.9] is an ordinary inhomogeneous differential equation of the first order for $A_{j\alpha(t)}$.

Define

$$B_{j\alpha} = \frac{1}{X_{j\alpha}} \int \frac{\mathcal{T} \cdot M^{*}_{j\alpha}}{gh} \, dA \qquad [4.10]$$

and the formal solution of [4.9] is

$$A_{j\alpha}(t) = \int_0^t B_{j\alpha}(\tau)\, e^{i\sigma_{j\alpha}(\tau - t)}\, d\tau . \qquad [4.11]$$

When the integrand on the right side of [4.9] is not a simple analytical function of time (which is the usual case) the time integration of [4.9] must be performed numerically. Although many methods exist for this purpose, a simple implicit procedure proves to be advantageous here. Let Δt represent the time increment for numerical integration. Approximate the time derivative in [4.9] by a central difference and average the other terms over the time step. That is

$$\frac{1}{\Delta t}\left[A_{j\alpha}(t + \Delta t) - A_{j\alpha}(t)\right] + \frac{i\sigma_{j\alpha}}{2}\left[A_{j\alpha}(t + \Delta t) + A_{j\alpha}(t)\right.$$

$$= \frac{1}{2}\left[B_{j\alpha}(t + \Delta t) + B_{j\alpha}(t)\right] \qquad [4.12]$$

where $B_{j\alpha}$ is as defined in [4.10]. After isolating $A_{j\alpha}(t + \Delta t)$ on the left side, [4.12] becomes

$$A_{j\alpha}(t + \Delta t) = \left[\frac{2 - i\sigma_{j\alpha}\Delta t}{2 + i\sigma_{j\alpha}\Delta t}\right] A_{j\alpha}(t) + \left[\frac{\Delta t}{2 + i\sigma_{j\alpha}\Delta t}\right]\left[B_{j\alpha}(t+\Delta t) + B_{j\alpha}(t)\right] \qquad [4.13]$$

This integration scheme has been investigated by Kurihara (1965) who showed that it is unconditionally stable for any choice of Δt but that phase errors may occur in the solution if Δt is larger than about one-sixth the period of the fastest wave in the system.

With knowledge of the structures of the normal modes, the normalization factors $X_{j\alpha}$ may be found by [4.6]. Since the forcing function $\hat{\mathcal{C}}$ is known at every time step, the $B_{j\alpha}$ in [4.13] can be evaluated by [4.10]. The frequencies, $\sigma_{j\alpha}$, of the normal modes are also known so that [4.13] represents a predictive equation for the time dependent expansion coefficients $A_{j\alpha}$. At each time step the transport and height fields are given by [4.7].

The preceding discussion of the normal mode method for solving the forced problem depends essentially on prior knowledge of the normal modes. Since these are determined numerically by the method in Chapter 3, the expansions [4.7] and integration [4.10] must also be performed numerically. Although the numerical calculations seem quite extensive, the ability to limit the range of the index α in [4.13] makes these calculations more efficient than space-time finite difference integrations. The next chapter illustrates this point by application of the normal modes method and comparison with space-time finite difference method.

CHAPTER FIVE

COMPARISON OF SOLUTIONS BY NORMAL MODE AND FINITE DIFFERENCE METHODS

In this chapter the normal mode method is tested against a finite difference method in two idealized situations. The finite difference method is similar to one used by Platzman (1972) in a resonance interation procedure for determining the free modes of oscillation of lakes. Results of the finite difference and normal mode calculations are compared for a rectangular basin of uniform depth subjected to uniform wind stress and for Lake Ontario with uniform wind.

A. The Finite Difference Method:

The governing equations [2.1] are discretized on the lattice shown in Figure 3. The horizontal coordinates are replaced by discrete coordinates $x_j = j\,\Delta_x/2$, $y_k = k\,\Delta y/2$ where j and k are integers. Note that the arrangement of variables on the grid allows the use of central differences for $\nabla \cdot \mathbf{M}$ at η-points, $\partial\eta/\partial x$ at M-points, and $\partial\eta/\partial y$ at N-points. To find N at M-points and vice versa for the coriolis terms a weighted average must be employed (see Platzman 1972). Define (at M-points)

$$\bar{N}_{j,k} = \frac{1}{8} F_{j,k} [(F_{j,k} + F_{j-1,\,k-1}) N_{j-1,k-1} + (F_{j,k} + F_{j-1,k+1}) N_{j-1,k+1} + (F_{j,k} + F_{j+1,k+1}) N_{j+1,k+1} + (F_{j,k} + F_{j+1,k-1}) N_{j+1,k-1}], \qquad [5.1]$$

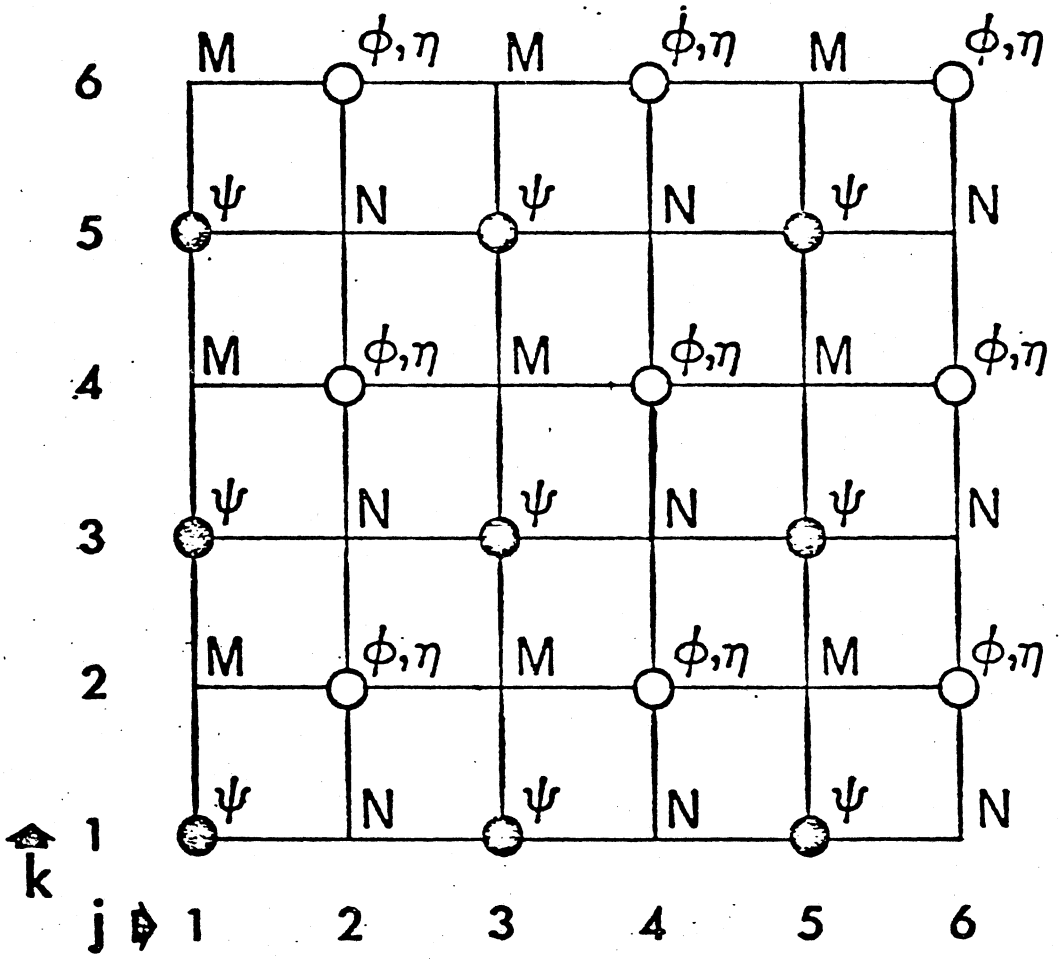

Figure 3. Distribution of variables on the numerical grid.

where the weighting factor $F_{j,k} \equiv f/h_{j,k}$ is the potential vorticity. The same sort of definition applies for $\overline{M}_{j,k}$ at N-points. $M_{j,k}$ and $N_{j,k}$ represent the discretized variables $M(x_j, y_k)$, $N(x_j, y_k)$. The equations are also discretized in time. Let the discretized time be given by $t_n = n\,\Delta t$ where n is an integer and Δt the time increment. Use a superscript to represent the time at which the discretized variables are to be evaluated. Represent the time derivatives in [2.1a] as a central difference at time $t_{n+\frac{1}{2}}$ and the time derivative in [2.1b] at t_n. Moving the predictive variables to the left side and rearranging the order of the equations results in the following system.

$$\eta^{n}_{j,k} = \eta^{n-1}_{j,k} - \frac{\Delta t}{\Delta x}\left(M^{n-\frac{1}{2}}_{j+1,k} - M^{n-\frac{1}{2}}_{j-1,k}\right) - \frac{\Delta t}{\Delta y}\left(N^{n-\frac{1}{2}}_{j,k+1} - N^{n-\frac{1}{2}}_{j,k-1}\right) \qquad [5.2a]$$

$$M^{n+\frac{1}{2}}_{j,k} = M^{n-\frac{1}{2}}_{j,k} + f\,\Delta t\,\overline{N}^{n-\frac{1}{2}}_{j,k} - \frac{g\,\Delta t}{\Delta x} h_{j,k}\left(\eta^{n}_{j+1,k} - \eta^{n}_{j-1,k}\right) + \Delta t\,\tilde{\tau}^{n+\frac{1}{2}}_{x\,j,k} \qquad [5.2b]$$

$$N^{n+\frac{1}{2}}_{j,k} = N^{n-\frac{1}{2}}_{j,k} - f\,\Delta t\,\overline{M}^{n+\frac{1}{2}}_{j,k} - \frac{g\Delta t}{\Delta y} h_{j,k}\left(\eta^{n}_{j,k+1} - \eta^{n}_{j,k-1}\right) + \Delta t\,\tilde{\tau}^{n+\frac{1}{2}}_{y\,j,k} \qquad [5.2c]$$

The value $\overline{M}^{n+\frac{1}{2}}_{j,k}$ appears to be an unknown in [5.2c] but it is actually known if [5.2b] is applied before [5.2c]. The numerical lattice is drawn so that the boundary is always a segment joining two ψ-points in Figure 3. In this way the boundary condition [2.2] is satisfied by setting $M_{j,k} = 0$ on a boundary parallel to the y-axis and $N_{j,k} = 0$ on a boundary parallel to the x-axis.

To a large degree of accuracy, the stability criterion for the system [5.2] may be approximated by

$$\Delta t \leq \frac{\Delta s}{\sqrt{2gh_o}} \qquad [5.3]$$

where Δs is the smaller of Δx, Δy and h_o is the maximum depth.

B. A Rectangular Basin Subject to Uniform Wind Stress:

The grid shown in Figure 3 is extended so that the maximum j and k values are both twenty-one. Depth is assumed constant. Dimensions of the basin are $L_x = 1.01\ L_y$. The grid intervals are $\Delta_x = L_x/10$, $\Delta_y = L_y/10$. The dynamical equations are non-dimensionalized by replacing M with $M/\sqrt{gh}\ L_x$, η with η/L_x, X with X/L_y, y with y/L_y and t with $t\sqrt{gh}/L_x$. The Coriolis parameter is chosen as the lowest frequency of a free mode of oscillation in the non-rotating basin, $\pi\sqrt{gh}/L_x$. This value of f represents a higher rate of rotation than that of most natural basins.

The normal modes of this basin are determined by the method discussed in Chapter 3. In the case of uniform depth, all the normal modes are gravitational (first class). A few of the non-dimensionalized periods are

presented in Table 2. The modes are numbered consecutively as the characteristic frequency of oscillation increases. The values of (k,l) represent the number of nodal lines perpendicular to the x- and y-axes for the corresponding mode in the absence of rotation.

Table 2. Periods of the six lowest modes in a 1 x 1.01 basin.

MODE (k,l)	PERIOD
1 (1,0)	2.81
2 (1,1)	1.55
3 (0,1)	1.34
4 (1,2)	.99
5 (2,0)	.96
6 (0,2)	.89

Since the lowest normal modes have the largest space scales, they are expected to acquire the most energy from a coordinated wind stress acting on the entire basin. Consequently, the range of the index α in the summation [4.7] is set at α max = 15. The normalization factors for the first fifteen modes are computed from [4.6]. Obviously $X_{1\alpha} = X_{2\alpha}$. The expression [4.10] for $B_{j\alpha}$ is independent of time for τ = constant and is determined once for all time. Since τ is a real quantity, $B_{1\alpha} = B^*_{2\alpha}$. It can also be shown that $A_{1\alpha} = A^*_{2\alpha}$. The time dependent expansion coefficients $A_{1\alpha}$ are then computed at each time step by repeated applications of [4.13]. The time increment is chosen as $\Delta t\sqrt{gh}/L_x = .07$ to satisfy the requirement for suppression of phase errors in the solution.

The solution obtained by the above procedure for four hundred time steps with $\tilde{\tau}_x = L_x\sqrt{gh}\,/L_y$, $\tilde{\tau}_y = 0$ is presented, in terms of the non-dimensional free surface displacement η/L_x at four points near the perimeter of the basin as the dashed line in Figures 4 and 5. Upper right represents $\eta_{20,20}$, center right $1/2(\eta_{20,12} + \eta_{20,10})$, lower right $\eta_{20,2}$, and lower center $1/2(\eta_{10,2} + \eta_{12,2})$. The solid line is the solution obtained by the finite difference scheme [5.2] with $\Delta t\sqrt{gh}/L_x = .07$, the maximum time step allowed by the stability criterion [5.3]. It is clear that there is excellent agreement between the two methods.

Despite the use of the same time step, the normal mode method required only 37% of the computation time for the finite difference solution. Two additional runs of the normal mode program were made, one with $\Delta t\sqrt{gh}/L_x = .035$, $\alpha\max = 15$ and the other with $\Delta t\sqrt{gh}/L_x = .07$, $\alpha\max = 30$. These changes had a negligible effect on the results. The two runs used 42% and 58% of the finite difference computation time respectively.

The normal modes in a rectangular basin of uniform depth are either symmetric or antisymmetric about the center of the basin, as shown by Rao (1966). For this reason some of the expansion coefficients $A_{j\alpha}$ should vanish since the $B_{j\alpha}$ computed from [4.10] are zero for the η-symmetric modes when $\tilde{\tau}$ = constant. The water level response of the rectangular basin to uniform wind stress is therefore antisymmetric about the center of the basin. The r.m.s. values of the $A_{1\alpha}$ are shown in the first column of Table 3 in Appendix A. All of the $A_{1\alpha}$ with zero value are associated with symmetric normal modes. The remainder correspond to antisymmetric modes. The

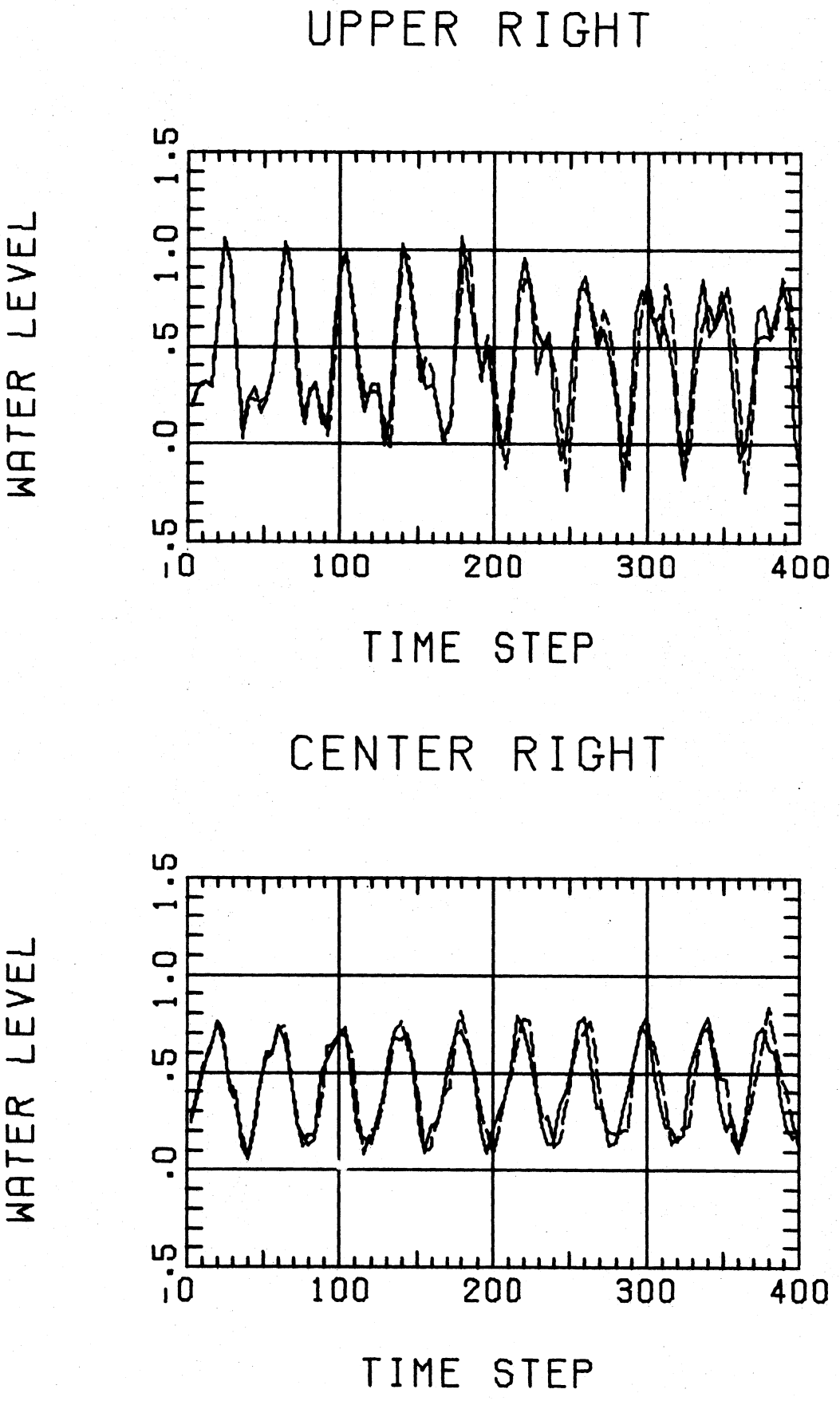

Figure 4. Comparison of normal mode (dashed) and finite difference (solid) solutions at two stations in a rectangular basin.

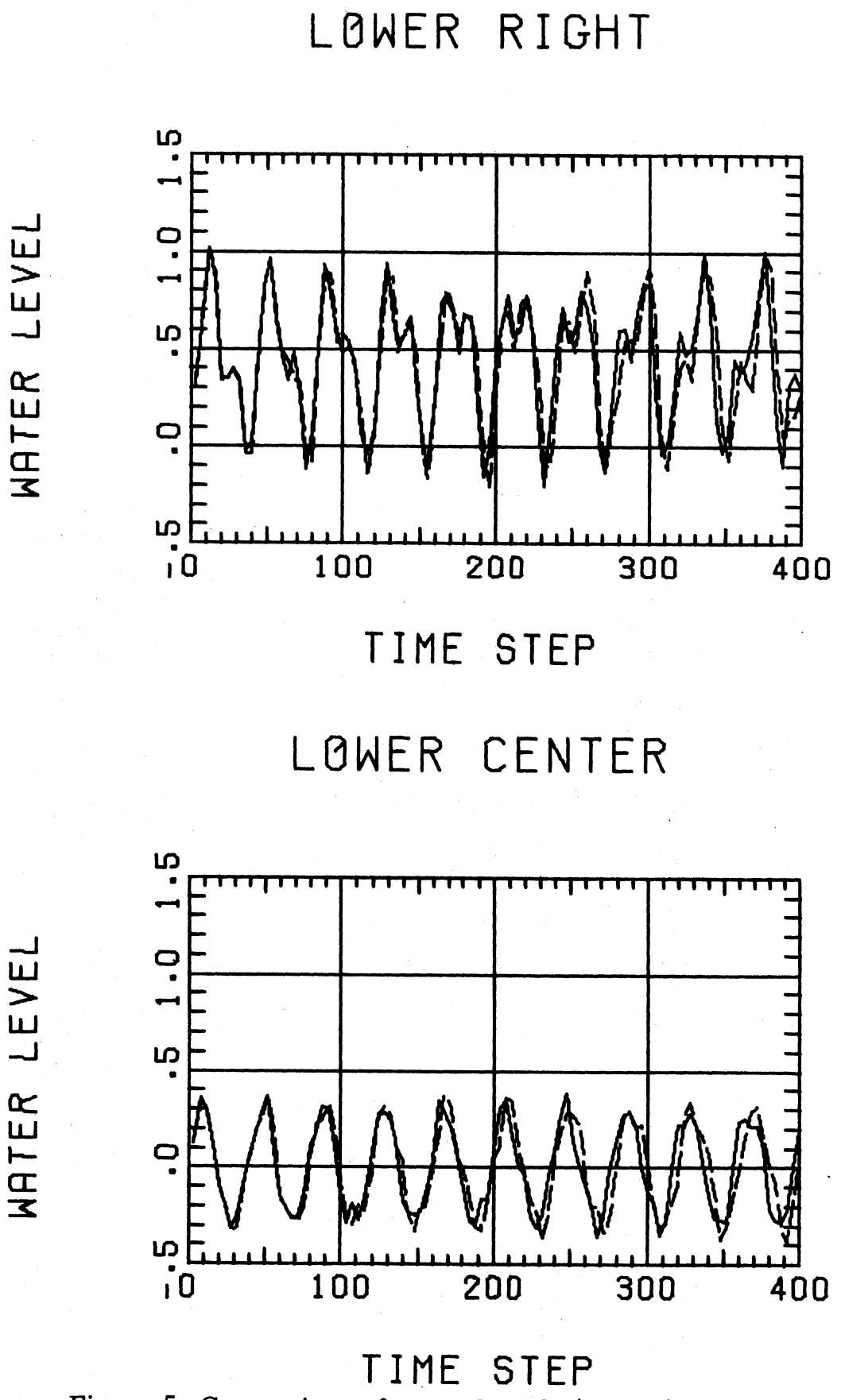

Figure 5. Comparison of normal mode (dashed) and finite difference (solid) solutions at two stations in a rectangular basin.

relatively large r.m.s. values of $A_{1\alpha}$ for the first and third modes explain the response of the basin. The most obvious periodic fluctuation of the water level in Figures 4 and 5 corresponds to the excitation of the [1, 0] mode. The periodicity associated with the secondary peaks in the water level fluctuation, which are seen at the corners of the basin and to a much lesser degree along the sides, can be attributed to the [0, 1] mode since its free surface response is largest at the corners and smallest along lines connecting the mid-points of the sides of the basin (see Rao 1966).

C. Lake Ontario Subject to Uniform Wind Stress:

In a basin of non-uniform depth both gravitational (first-class) and rotational (second-class) normal modes are possible. The gravitational modes form a sequence with periods decreasing from the largest and approaching zero as indicated for Lake Ontario by Table 1. In Lake Ontario the smallest period calculated for the spectrum of rotational modes by Rao and Schwab (1974) is 52 hours. Since the time scale of a storm surge is generally not this long, only the spectrum of gravitational modes for Lake Ontario is considered.

The pertinent physical constants for Lake Ontario are $g = 9.8$ m/sec and $f = 10^{-4}$/sec. The numerical grid shown in Figure 6 is the one used by Rao and Schwab (1974). The grid intervals are $\Delta x = \Delta y = 10.08$ km. This grid is used here for both finite difference and normal mode methods. The forcing acts along the x-axis at a relatively strong value of $\tilde{\tau}_x = 3$ cm^2/sec^2 for 96 hours. The time step for the integration [4.13] in the normal mode

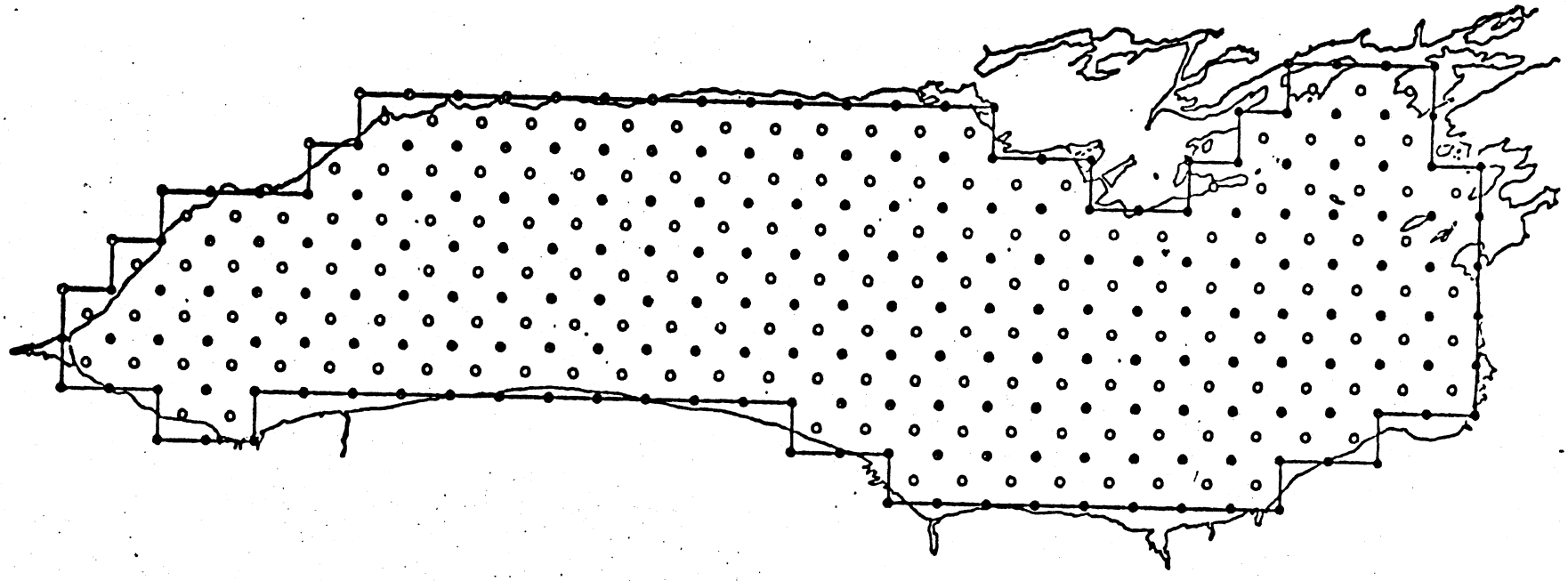

Figure 6. Numerical grid on Lake Ontario.

method has been chosen as 10 min. with αmax = 15, in order to prevent phase errors in the solution. The stability criterion [5.3] for the finite difference method requires $\Delta t \leq 2.5$ min for a maximum depth h_o = 225 m. The time step used here is 2 min.

The results of the normal mode and finite difference computations were compared at the nearest grid point to stations S1 - S10 in Figure 7. The water level fluctuation at four representative stations is shown in Figures 8 and 9. The solid line represents the finite difference solution and the dashed line the solution by the normal mode method. Careful scrutiny of the finite differences result at Cape Vincent in Figure 9 reveals a slow fluctuation with a period of about 50 hours that is not present in the normal mode solution. This effect could be due to the excitation of rotational normal modes. The rotational modes may play an important role in long-term calculations but for the prediction of storm surges the small amplitude of this oscillation indicates that there is ample justification for restricting the normal mode spectrum to gravitational modes.

Since the time increment for the normal mode method is five times the value for the finite difference calculations, the savings in computation time are quite large. The normal mode method required only 5.4% of the finite difference computation time. The normal mode method was also applied with αmax = 30, Δt = 10 min. and α max = 15, Δt = 5 min. The effect of using more normal modes or decreasing the time step was negligible.

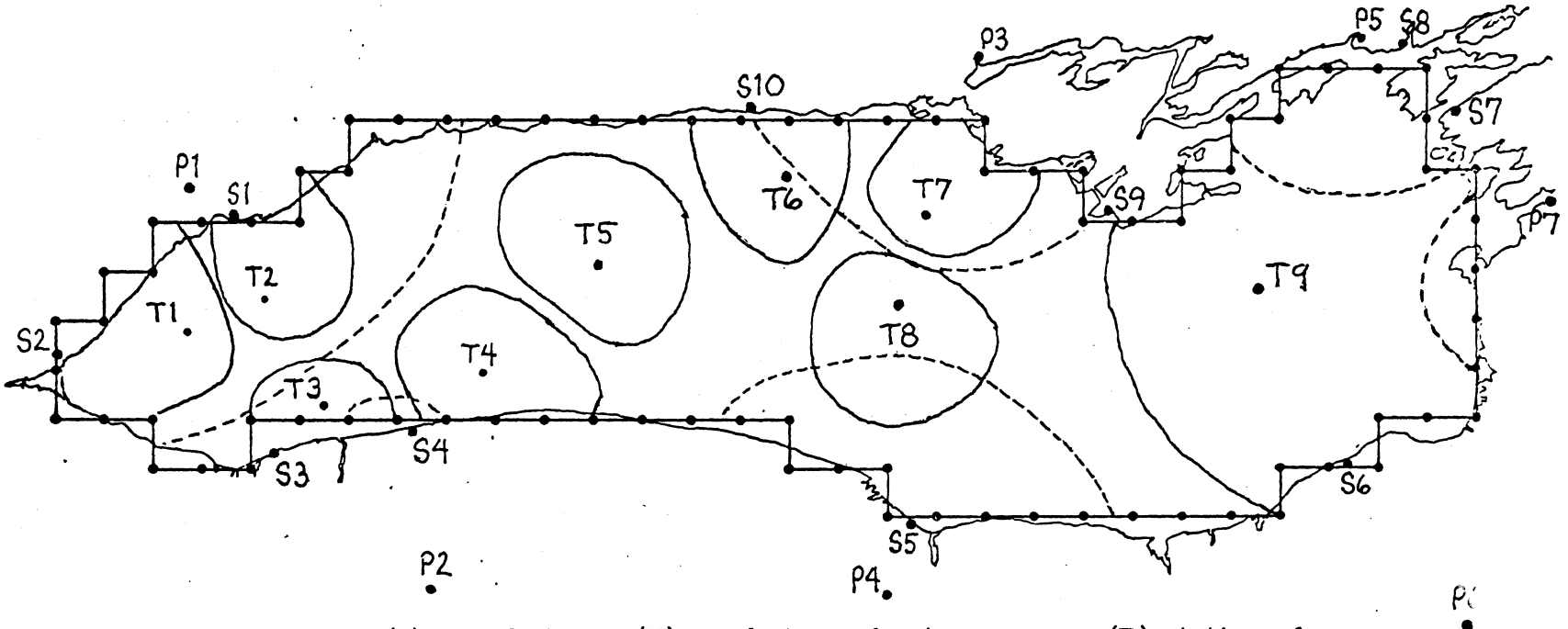

Figure 7. Location of water level (S), wind stress (T), and atmospheric pressure (P) stations for Lake Ontario.

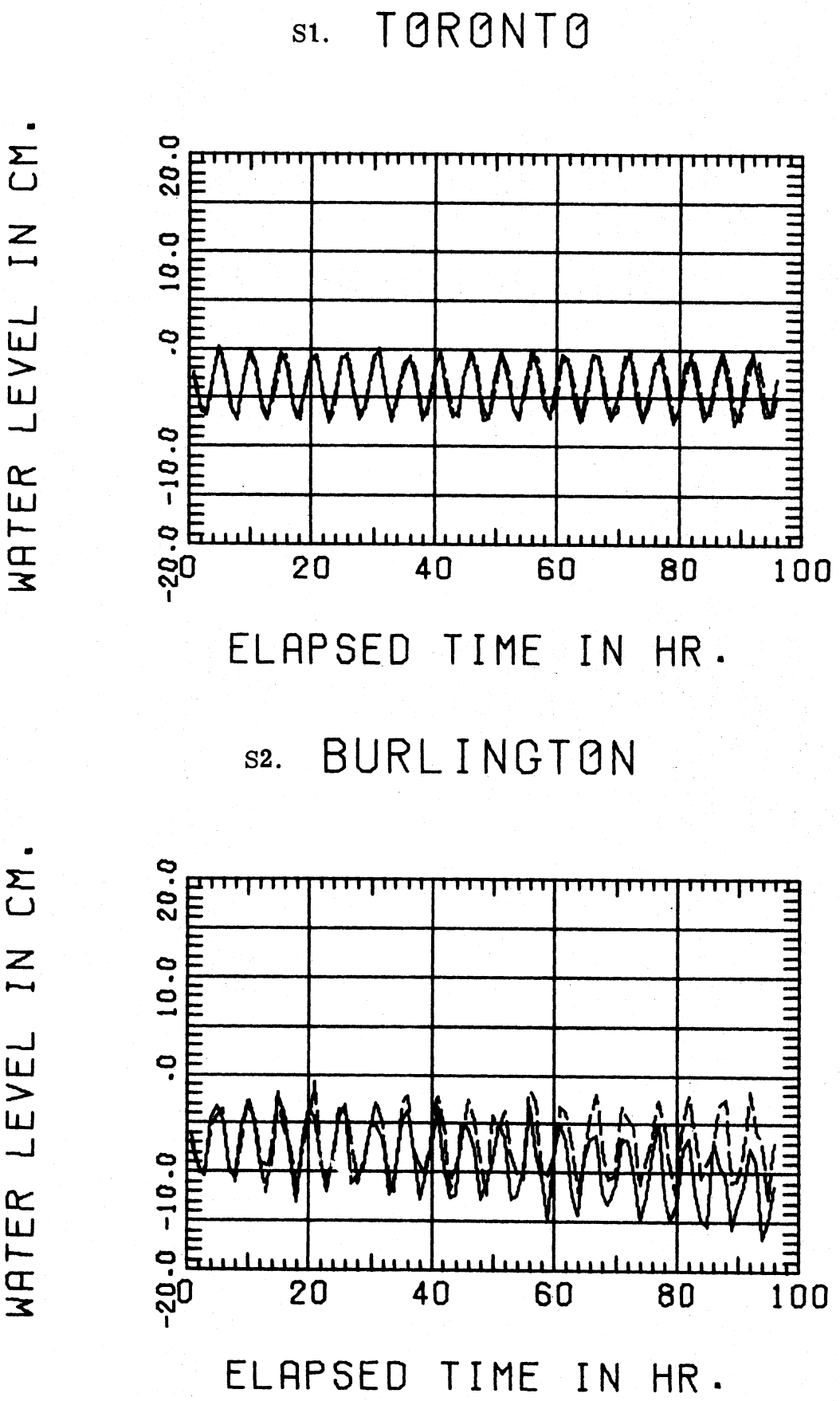

Figure 8. Normal mode (dashed) and finite difference (solid) solutions for Lake Ontario with uniform wind.

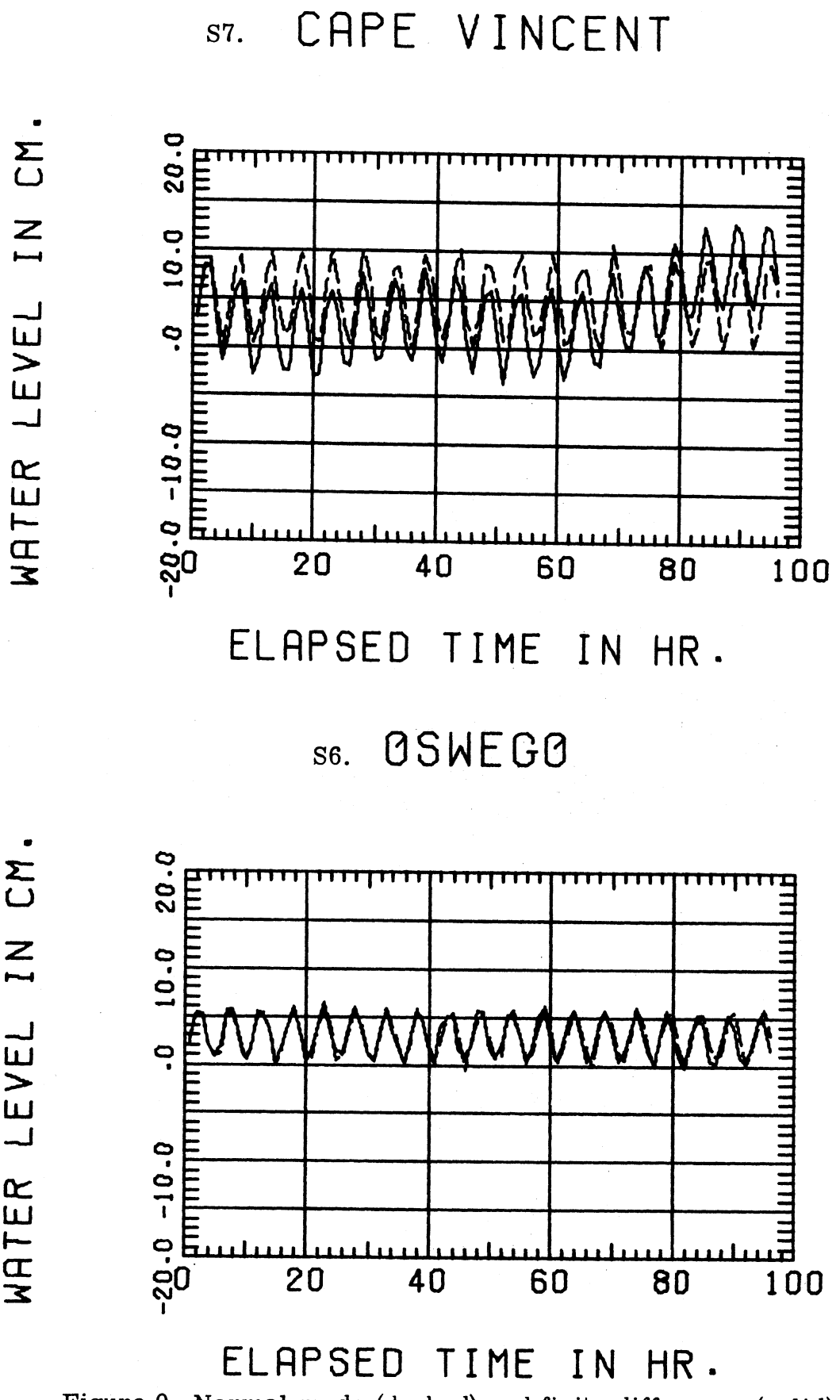

Figure 9. Normal mode (dashed) and finite difference (solid) solutions for Lake Ontario with uniform wind.

The dominance of the first normal mode in the response of the lake is evident in Figures 8 and 9. The second column of Table 3 in Appendix A explains this phenomenon. The mode with the next largest expansion coefficient to the first is the fourth mode with less than twenty percent of the r.m.s. value of the first. The normal modes of Lake Ontario are not strictly symmetric or antisymmetric as is the case in a rectangular basin so that any mode may acquire energy from a uniform wind stress.

The normal mode method is at least as accurate as the finite difference method and much more efficient computationally for the natural topography of Lake Ontario subject to ideal wind stress. The next chapter presents results of the normal mode method with natural wind stress.

CHAPTER SIX

APPLICATION TO A STORM ON LAKE ONTARIO

The final test of the normal mode method is an application to a natural storm surge episode. The necessary atmospheric and hydrographic data for simulating a natural episode have been made available through the efforts of participants in the International Field Year on the Great Lakes. The water level, atmospheric pressure, and wind stress data cover the passage of tropical storm Agnes along the eastern edge of Lake Ontario during the latter half of June, 1972. This chapter analyzes the results obtained by application of the normal mode method to the episode and compares the results with observed data.

Wind stress data has been supplied by the Canada Centre for Inland Waters for the period of 16 June to 10 July 1972. The data represents hourly averages of the stress computed from ten-minute readings at stations labeled T1-T9 in Figure 7. In an operational situation the wind stress data is not available in advance but must be inferred from geostrophic or gradient winds computed from atmospheric predictions. The purpose here is to test the performance of the normal mode method without consideration of the applicability of geostrophic or gradient winds, thus the use of observed wind stress is warranted.

The wind data supplied at each station is the hourly average of the wind velocity squared. Wind stress is defined as

$$\tau^{\omega} = \rho_{\omega} c_o |w_a| w_a \qquad [6.1]$$

where $c_o = \frac{\rho_a}{\rho_\omega} K$ is the ratio of the density of air to the density of water times a dimensionless skin friction coefficient K. In [6.1] w_a is the vector wind velocity at 10 m. anemometer level. An acceptable value of c_o for the prediction of storm surges is $c_o = 3 \times 10^{-6}$ which is adopted here. This value of c_o was found to give the best agreement between computed and observed water levels.

The atmospheric pressure data supplied at three hourly intervals for stations P1-P7 in Figure 7 indicate that during storm Agnes the difference in atmospheric pressure between the eastern and western ends of Lake Ontario amounted to as much as 10 mb. This difference represents a hydrostatic difference in water level of about 10 cm. Variations of the water level at most stations around the lake during this episode were seldom more than twice this large. Therefore, the effect of atmospheric pressure gradients must also be considered.

The external forcing function τ in the dynamical equations [2.1] can be represented as

$$\tau = \rho_{\omega}^{-1} \tau^{\omega} - \rho_{\omega}^{-1} \nabla P \qquad [6.2]$$

where P is the atmospheric pressure. The equations require that τ be a prescribed function of x, y, and t. Since available wind stress and atmospheric pressure are prescribed only at discrete locations, some spatial interpolation scheme must be employed. Let the discrete value of wind stress and atmospheric pressure be τ^{ω}_{m} and P_m where the subscript m represents the individual stations. Define continuous influence functions $I_m(x,y)$, $J_m(x,y)$ for each station so that

$$\tau^{\omega}(x,y,t) = \sum_m I_m(x,y)\,\tau^{\omega}_{m}(t)$$

$$P(x,y,t) = \sum_m J_m(x,y)\,P_m(t). \qquad [6.3]$$

The interpolation functions I_m and J_m are computed in the following manner. Define

$$a_m(x,y) = (x-x_m)^2 + (y-y_m)^2, \qquad [6.4]$$

the square of the distance between point (x, y) and station m. Further, define

$$b_m(x,y) = \prod_{n \neq m} a_n(x,y), \qquad [6.5]$$

the product of all a_n except a_m. Then

$$I_m(x,y) = b_m(x,y)/\sum_m b_m(x,y). \qquad [6.6]$$

The influence function I_m has the following properties:

$$I_m(x_n, y_n) = \begin{cases} 1 \text{ if } m = n \\ 0 \text{ if } (x_n, y_n) \text{ represents a different station } n. \end{cases}$$

$$\sum_m I_m(x, y) = 1. \qquad [6.7]$$

The same procedure is used to establish $J_m(x, y)$. This type of influence function has been used successfully by Platzman (1963). The area around each wind stress station for which $I_m > .5$ is enclosed by a solid line in Figure 7. The area for which $J_m > .5$ around the atmospheric pressure stations is indicated by a dashed line.

To apply the normal mode method to the Agnes episode, the fifteen lowest gravitational modes are included for the reasons stated in Chapter 5. The $B_{j\alpha}$ in [4.13] are time dependent for time dependent wind stress and are found in the following way:

$$B_{j\alpha}(t) = \frac{1}{X_{j\alpha}} \int \frac{\mathcal{T} \cdot M^*_{j\alpha}}{gh} dA$$

$$= \frac{1}{X_{j\alpha}} \int \frac{(\mathcal{T}^{\omega} - \nabla P) M^*_{j\alpha}}{\rho \omega g h}$$

$$= \frac{1}{\rho \omega g X_{j\alpha}} \int h^{-1} \left(\sum_m I_m(x, y) \mathcal{T}^{\omega}_m(t) - \nabla \sum_m J_m(x, y) P_m(t) \right) \cdot$$

$$\lfloor M^*_{j\alpha} dA = \sum_m \frac{\mathcal{T}^{\omega}_m(t)}{\rho \omega g X_{j\alpha}} \cdot \int h^{-1} I_m(x, y) \lfloor M^*_{j\alpha} dA$$

$$- \sum_m \frac{P_m(t)}{\rho \omega g X_{j\alpha}} \int h^{-1} \nabla J_m(x, y) \cdot \lfloor M^*_{j\alpha} dA. \qquad [6.8]$$

Now the evaluations of the integrals in [6.8] over the area of the basin can be done numerically once for all time. At each time step $B_{j\alpha}$ is computed by summing the vector product of the wind stress and the first integral for all

the wind stress stations then subtracting the product of atmospheric pressure and the second integral summed over all the atmospheric pressure stations.

Peak wind stress and pressure gradients occurred between 0:00 and 6:00 GMT on June 23. Wind stress was generally directed towards the southwest with amplitude as high as 6 cm^2/sec^2. The iteration scheme [4.13] for the expansion coefficients $A_{j\alpha}$ has been applied from 0:00 GMT 22 July to 0:00 GMT 24 July with a time step Δt = 10 min. Wind stress and atmospheric pressure data are interpolated from their hourly and three hourly values respectively for evaluation of $B_{j\alpha}$ by [6.8] at each time step. The results for the water level have been compared to observed variations of the mean level at the ten stations (S1-S10) around the lake. The observed values represent instantaneous hourly readings, not averages. Four representative comparisons are presented in Figures 10 and 11.

The maximum water level displacements predicted by the normal mode method at the various stations agree quite well with the observed values except at Burlington. This discrepancy at Burlington is probably due to discretization errors in the numerical grid at the western end of the lake. The most obvious difference between computed and observed water level variations at all stations is the consistent time lag of the computed values. The same sort of effect was noticed in computations for Lake Erie by Platzman (1963). He found that in the case of easterly winds there was an appreciable time lag from the peak water levels to the peak observed winds at the station with the most extensive influence function because this station was located in the northwestern part of the basin. The location and large

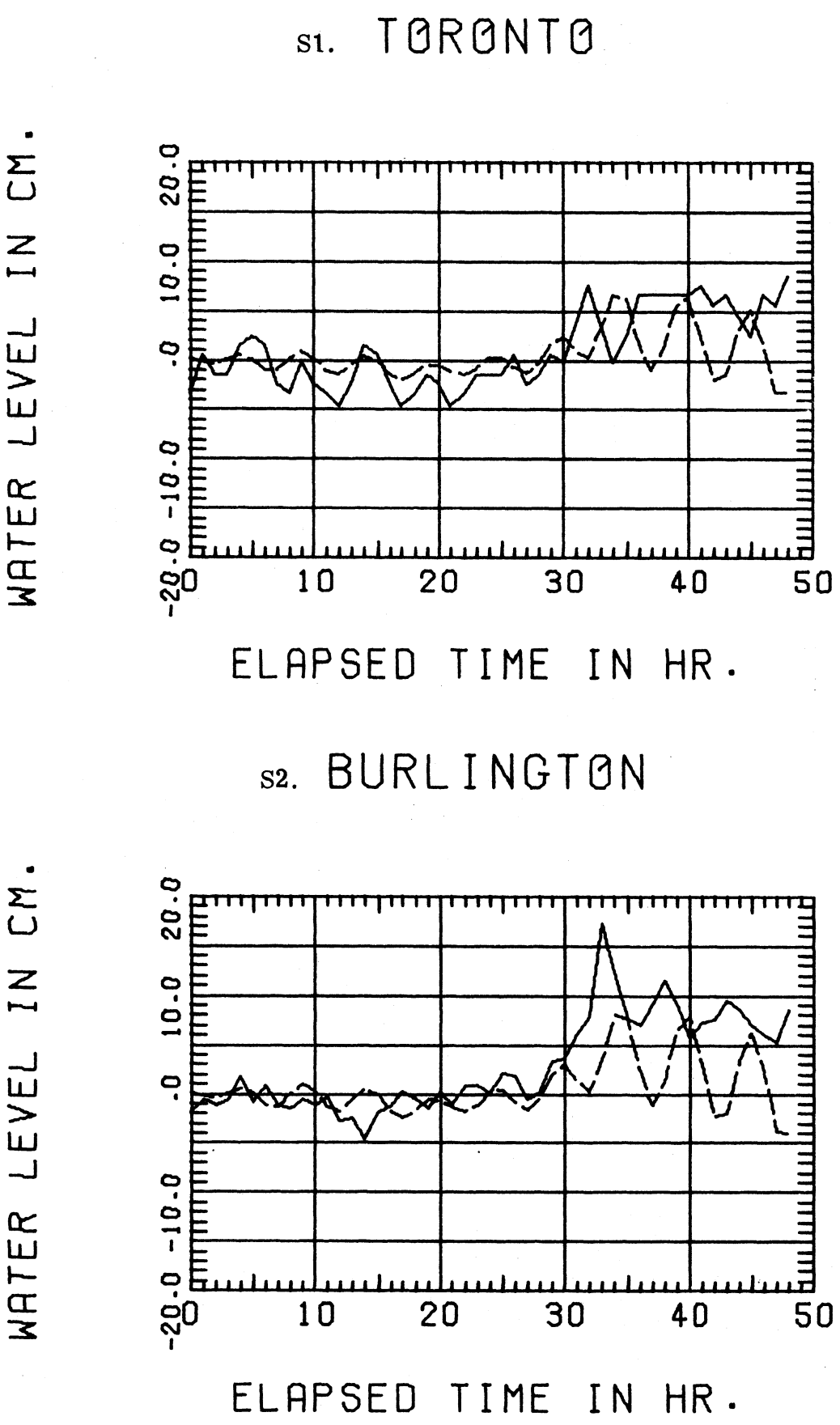

Figure 10. Computed (dashed) and observed (solid) variations in water level during Storm Agnes.

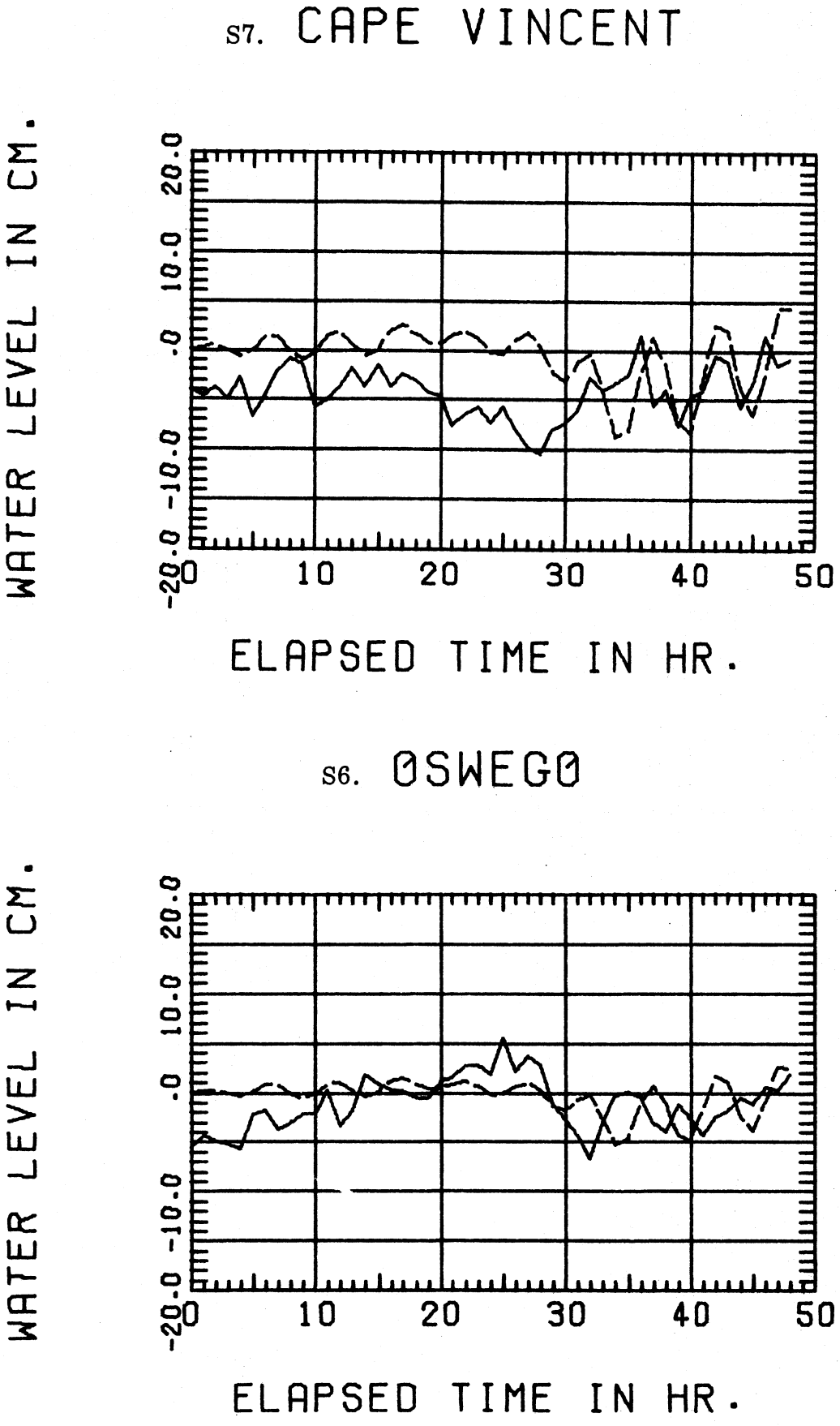

Figure 11. Computed (dashed) and observed (solid) variations in water level during Storm Agnes.

region of influence of station T9 in Figure 7 are probably producing an analogous effect since the strongest winds during Agnes were northeasterly. Apart from the phase lag, the principal resurgences at five and ten hours after the first surge due to excitation of the lowest normal mode (period 5.11 hours) are predicted quite well.

The third and fourth columns of Table 3 in Appendix A indicate that the lowest normal mode dominates the response of the lake, as it did for constant wind stress. The third column represents the r.m.s. values of $A_{j\alpha}$ for the day before the storm. In the fourth column are the values for the following day. Each of the lowest five modes gained considerable energy from the passage of the storm. Percentagewise, the largest increases are for the third and fourth modes. The second mode appears to play a much more important role in a natural situation than it does for constant wind stress along the axis of the lake. The values of $A_{j\alpha}$ justify the assumption that the response of the lake is governed by the lowest modes.

Recently, Simons (1974) applied his multi-layered finite difference model to the Agnes episode. His results are presented in Figure 12. A low-pass digital filter was applied to both computed and observed water level fluctuations. A similar filter has been applied to the water level fluctuations predicted by the normal mode method at the same stations and the results are compared to the filtered observed values in Figures 13 and 14. The grid in Simons' model has twice the resolution of the grid employed here which may account for the larger fluctuation predicted by his model at Burlington. For some reason the filtered values of observed water levels

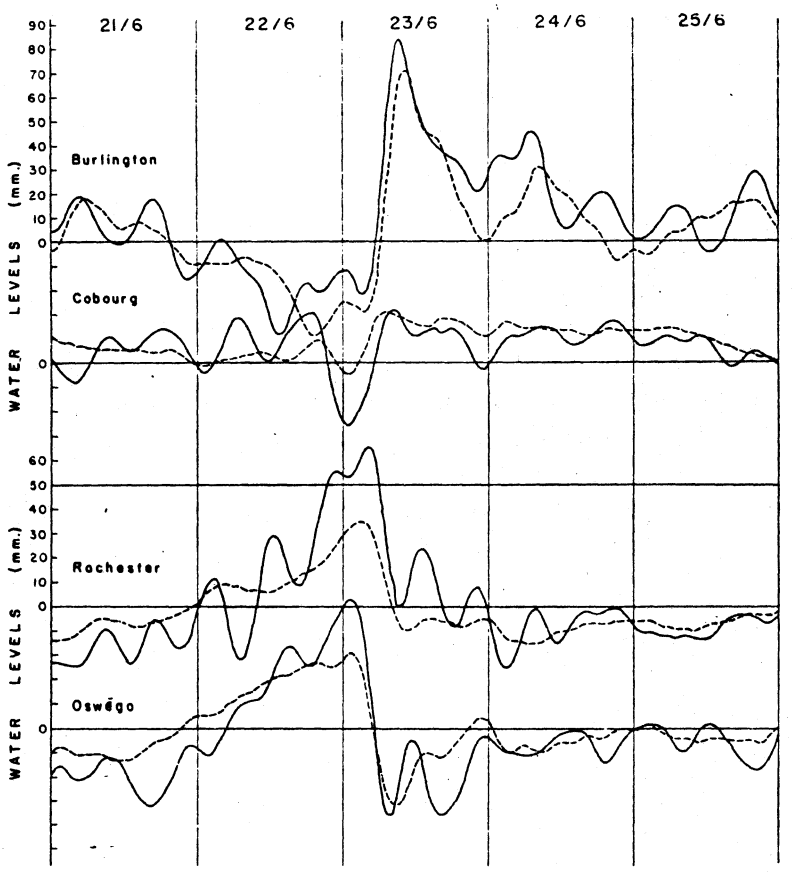

Figure 12. Computed (dashed) and observed (solid) water level variations during Storm Agnes. Time series are filtered to remove periods $\lesssim$ 5 hours (from T. J. Simons 1974).

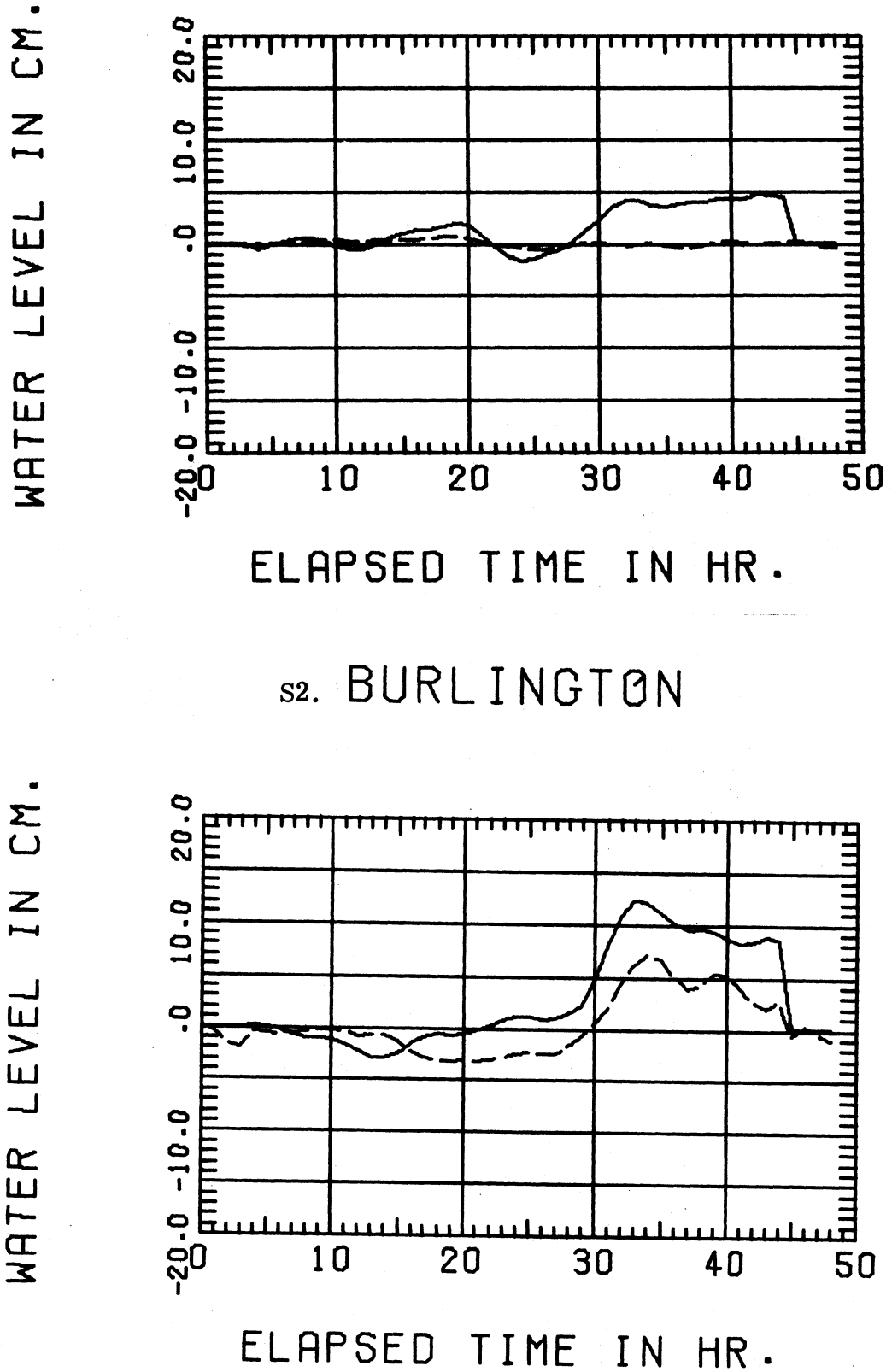

Figure 13. Computed (dashed) and observed (solid) water level variations during Storm Agnes. Time series are filtered to remove periods < 5 hours.

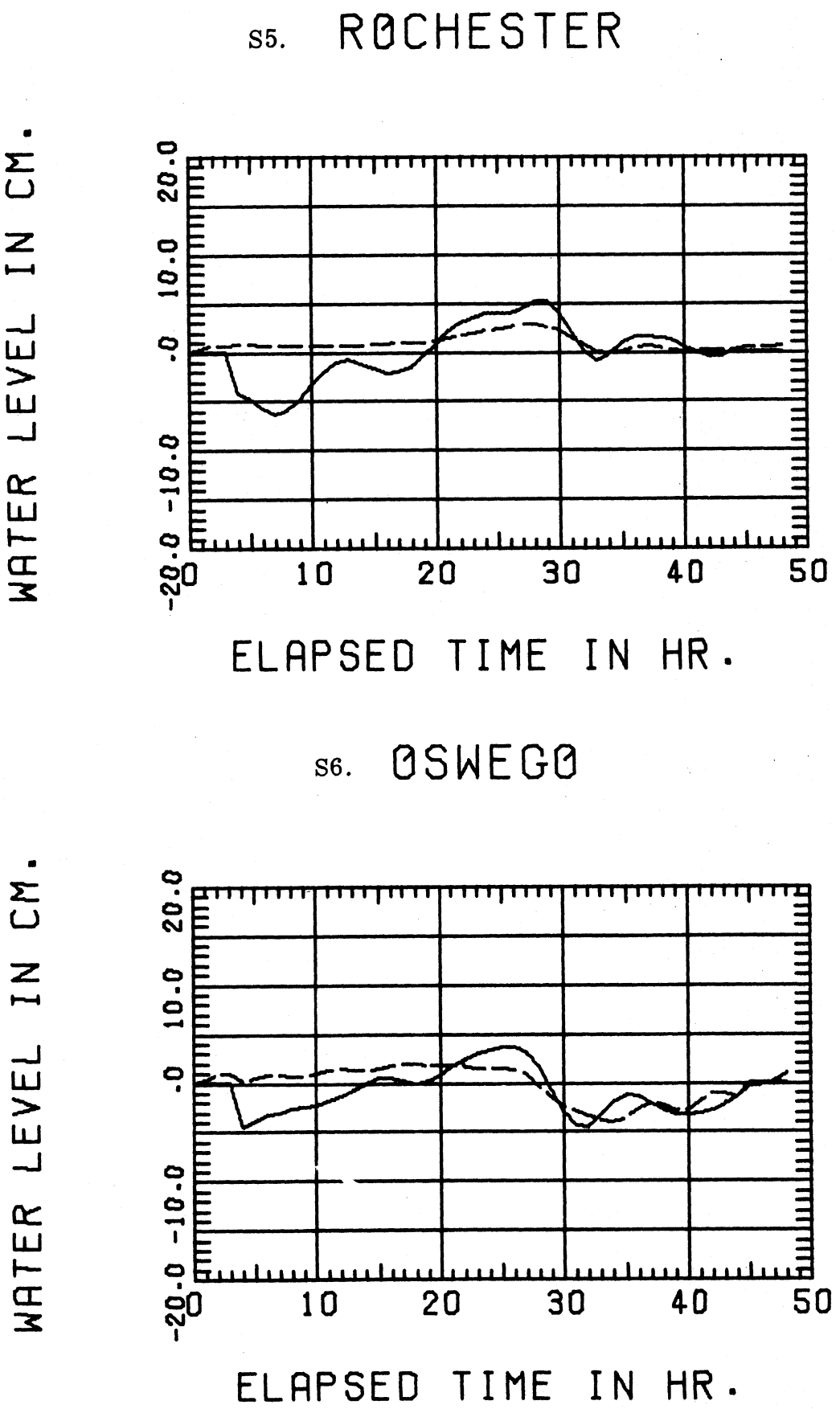

Figure 14. Computed (dashed) and observed (solid) water level variations during Storm Agnes. Time series are filtered to remove periods $\leq$ 5 hours.

at Coburg in Figure 13 are much larger than those in Figure 12. The computed values of 1-2 cm are similar in both figures. At Rochester and Oswego the normal mode method predicts values very similar to Simons' model.

It should be mentioned that during storm Agnes the only observed water level fluctuations greater than 20 cm was at Port Weller where the fluctuation exceeded 30 cm in just a few hours. This anomalous behavior represents either an inaccurate observation or a much smaller scale effect than a whole basin model could predict. Fluctuation at most stations was less than 10 cm. In this respect, the Agnes episode is not a representative storm surge. This episode was used as a verification for the normal mode method simply because of the availability of the data. Since the numerical model is designed to predict large water level displacements, it is expected that better results can be obtained when the free surface of the lake exhibits a more pronounced fluctuation. Even in this context, the results obtained during the Agnes episode by the normal mode method are quite encouraging.

CHAPTER SEVEN

CONCLUSIONS

The normal mode method has been applied to some idealized cases and the results have been compared with results of a finite difference method. The normal mode method proved to be at least as accurate and much more efficient than the finite difference method. In some applications, the normal mode method required only 5% of the finite difference computation time. In an example of a natural storm surge episode, the normal mode method predicted water level fluctuations quite well even though some time lag between observed and computed values is present. The results compare well with those obtained by a finite difference model with twice the grid resolution. The ability to limit the spectrum of normal modes included in the time integration of the dynamical equations may be used in the future to apply the method to long-term prediction by inclusion of rotational mode spectrum.

REFERENCES

Hamblin, P. F. 1972. Some free oscillations of a rotating natural basin. Univ. Washington, Dept. Oceanography, Ph.D. Thesis, 97 p.

Kurihara, Y. 1965. On the use of implicit and iterative methods for the time-integration of the wave equations. Monthly Weather Review, 93: 33-46.

Lamb, H. 1932. Hydrodynamics, 6th ed., Cambridge Univ. Press, 738 p.

Lauwerier, M. A. 1961. The North Sea Problem VI. Nonstationary wind effects in a rectangular bay. (Theoretical Part). Proc. Koninklijke Nederlandske Akad. Van Wettenschappen, Series A, 64: 104-122.

_____ and B. R. Damste. 1963. The North Sea Problem VIII. A numerical treatment. Proc. Koninklijke Nederlandske Akad. Van Wettenschappen, Series A, 66: 167-184.

Platzman, G. W. 1958. A numerical computation of the surge of June 26, 1954 on Lake Michigan. Geophysica 6: 407-438.

_____ 1963. The dynamical prediction of wind tides on Lake Erie. Meteor. Monogr. 4(26): 44 p.

_____ 1972. Two dimensional free oscillations in natural basins. J. Phys. Oceano., 2: 117-138.

_____ 1974. Normal modes of the Atlantic and Indian Oceans. Tech. Rept. No. 25, Univ. Chicago, Dept. Geophysical Science, 83 p.

Proudman, J. 1953. Dynamical Oceanography. J. Wiley & Sons, 409 p.

Rao, D. B. 1966. Free gravitational oscillations in rotating rectangular basins. J. Fluid Mech., 25: 523-555.

_____ 1967. Response of a lake to a time-dependent wind stress. J. Geophys. Res., 72: 1697-1708.

_____ 1974. Transient response of shallow enclosed basins by the method of normal modes. Sci. Ser. No. 38, Canada Centre for Inland Waters, [in press].

_____ and D. J. Schwab. 1974. Two-dimensional normal modes in arbitrary enclosed basins on a rotating earth: application to Lakes Ontario and Superior. Spec. Rept. No. 19, Center for Great Lakes Studies, Univ. Wisconsin--Milwaukee, 69 p.

Reid, R. O. 1958. Effect of coriolis force on edge waves. (1) Investigation of normal modes. J. Mar. Res., 16: 109-141.

Simons, T. J. 1971. Development of numerical models of Lake Ontario. Proc. 14th Conf. Great Lakes Res., 655-672.

_____ 1973. Development of three-dimensional numerical models of the Great Lakes. Sci. Ser. No. 12, Canada Centre for Inland Waters, 26 p.

_____ 1974. Verification of numerical models of Lake Ontario: Part I. Circulation in spring and early summer. J. Phys. Oceano., 4: 507-523.

Welander, P. 1961. Numerical prediction of storm surges. In: Geophys., 8: 315-379.

APPENDIX A

Table 3. R.M.S. values of expansion coefficients.

	Rectangular basin with uniform wind stress	Lake Ontario with uniform wind stress	Lake Ontario during Storm Agnes: June 22	Lake Ontario during Storm Agnes: June 23
1.	.0229	.366	.363	.566
2.	.000	.033	.123	.214
3.	.0150	.021	.034	.104
4.	.0038	.061	.022	.083
5.	.0000	.017	.025	.051
6.	.0000	.024	.036	.037
7.	.0010	.048	.040	.056
8.	.0000	.026	.027	.050
9.	.0010	.023	.031	.043
10.	.0031	.009	.044	.063
11.	.0000	.009	.012	.025
12.	.0000	.013	.013	.017
13.	.0003	.001	.016	.026
14.	.0003	.016	.053	.058
15.	.0000	.004	.008	.009

APPENDIX B

COMPARISON OF TWO-DIMENSIONAL AND CHANNEL SOLUTIONS FOR LAKE ONTARIO WITH UNIFORM WIND STRESS

The topography of Lake Ontario may be approximated by a one-dimensional channel with varying cross-sectional area. This approximation allows one to describe the response of the lake to stress along the channel axis in terms of a one (space)-dimensional system of equations. The channel equations may be written as

$$\frac{\partial Q}{\partial t} = -gS \frac{\partial \eta}{\partial X} + b\tau$$

$$\frac{\partial \eta}{\partial t} = -\frac{1}{b} \frac{\partial Q}{\partial X} \qquad [B.1]$$

where $Q(x, t)$ is the volume transport through a vertical section of the channel, $\eta(x, t)$ is the free surface displacement across the section, $S(x)$ is the cross-sectional area, $b(x)$ is the surface breadth of the section, and $\tau(x)$ is the stress in the x-direction. The x-axis is taken as the local tangent to the main axis of the channel, increasing from west to east for Lake Ontario.

The system of channel equations does not take into account the effect of the earth's rotation or variations across the channel. The effect of the earth's rotation may be accounted for by imposing Kelvin wave dynamics on the longitudinal flow field. This implies a quasi-geostrophic perturbation to the free surface displacement field whose variation across the channel produces a pressure gradient which balances the effect of the Coriolis force. If the perturbation is $\eta(x)$, then

$$\frac{\partial \eta}{\partial y} = - \frac{fQ}{gS} \qquad [B.2]$$

When integrated across a section of the channel, [B.2] becomes

$$\eta_N - \eta_S = - \frac{bfQ}{gS} \qquad [b.3]$$

Where η_N and η_S are the perturbation on the north and south shores, respectively. If the perturbation is assumed to be equally distributed between the north and south shores ($\eta_N = -\eta_S$) then it may be expressed as

$$\eta_N = -\eta_S = - \frac{bfQ}{2gS} \qquad [B.4]$$

The derivatives in [B.1] are approximated by central differences at 51 equally spaced points along the axis of Lake Ontario in the following way

$$Q_j^{n+1} = Q_j^{n-1} - g\frac{S_j \Delta t}{2\Delta X}(\eta_{j+1}^n - \eta_{j-1}^n) + \frac{\Delta t \tau_j}{2}(b_{j-1} + b_{j+1})$$

$$\eta_j^{n+1} = \eta_j^{n-1} - \frac{\Delta t}{2b_j \Delta X}(Q_{j+1}^n - Q_{j-1}^n). \qquad [B.5]$$

Here Δt is the incremental time (4 min in this case) and ΔX the incremental distance (6 km). Superscripts denote time steps and subscripts denote space steps (i.e. $Q_j^n \equiv Q(j\Delta X, N\Delta t)$). The boundary condition is $Q_0 = Q_{52} = 0$. The wind stress is taken as a constant 3 cm^2/sec^2 and the equation [B.5] are applied at the appropriate incremental points along the channel axis for 96 hours. The result is shown as the solid line in Figure 15 in terms of the free surface displacement plus the quasi-geostrophic perturbation [B.4] for two representative stations on the shore of the lake. The dashed line is the solution obtained by the two-dimensional normal mode method. The magnitudes of the disturbances agree very well, but the frequency of oscillation in the channel solution is greater than in the two-dimensional case. This is because the frequency of the lowest free mode of oscillation (which dominates the response of the lake to uniform westerly wind as shown in Chapter 5, Section C) is higher in the channel case where no account is taken of the earth's rotation or two-dimensional effects. Despite the frequency difference, the channel equations are valuable as a simple tool for calculating the response of Lake Ontario to a stress along its axis.

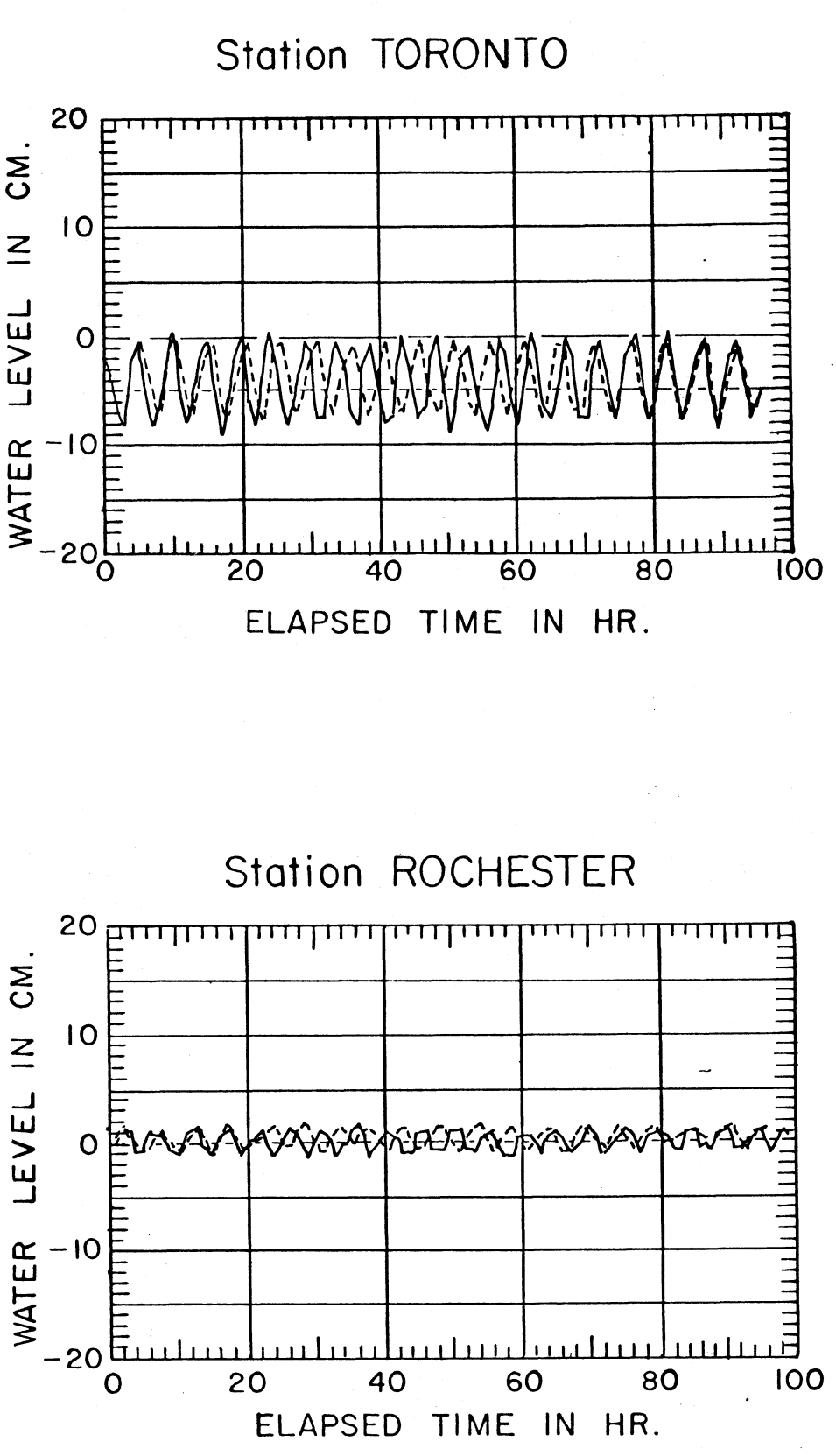

Figure 15. Responses of the free surface at two stations to a steady wind stress of 3 cm^2/sec^2 applied for 96 hr: unbroken line, computed using the channel equations with the quasi-geostrophic perturbation B. 4 imposed; broken line, computed using the two-dimensional normal mode method.